P148620.PDF [Page: 3 of 89]

94-619

COMMUNICATIONS
RESEARCH
LABORATORY

HIGH ACCURACY DIRECTION FINDING TRIALS

by

Titus Lo
Fengzhen Wang
John Litva

Faculty of Engineering
McMaster University
Hamilton, Ontario
Canada L8S 4K1

CRL Report No. 273
November 1993

P148620.PDF [Page: 4 of 89]

HIGH ACCURACY DIRECTION FINDING TRIALS

Titus Lo
Fengzhen Wang
John Litva

Communication Research Laboratory
McMaster University

Final Report for
Defence Research Establishment Ottawa
Under Contract No. W7714-2-9641

Scientific Authority: William J.L. Read

Abstract

This report is a part of the ongoing research that has been carried out by DREO and CRL to study the multipath effects on a direction finding (DF) system. The present project has been to establish a real DF database and to carry out a comprehensive analysis of the data. A highly advanced eight-element DF system has been used to collect field trial data. Based on the collected data, the development of signal model and the study of the characteristics of the multipath signals were carried out . Furthermore, a number of direction-of-arrival algorithms have been investigated and their performance has also been evaluated based on the real data. This report consists of the following parts:

1. experimental trials
2. signal modelling
3. data calibration
4. analysis of signal characteristics
5. development and investigation of practical techniques for direction finding
6. DF performance evaluation.

Based on the observations and findings during the course of this work, a number of recommendations are made for future research.

P148620.PDF [Page: 6 of 89]

Contents

1 Introduction **7**

2 Measurements **9**

2.1 The Measurement System 9

2.2 One-Source Measurements 9

2.3 Two Source Measurements 10

2.4 Mobile Source Measurements 10

3 Signal Modelling **13**

4 Data Calibration **17**

5 Analysis of Signal Characteristics **22**

6 DF Algorithms **29**

6.1 DFT 29

6.2 MUSIC 29

6.3 Spatio-temporal Estimation 31

6.4 Two-step Prediction Direction Finding 34

7 Analysis Results **38**

7.1 Typical Results 38

7.2 Performance Analysis 40

7.3 Mobile Trials 47

7.3.1 Case 1 47

7.3.2 Case 2 47

P148620.PDF [Page: 7 of 89]

7.3.3 Case 3 51
7.3.4 Case 4 52
7.3.5 Discussion 52

8 Conclusions and Recommendations 60

8.1 Findings 60
8.2 Recommendations 61

A Results of Multipath Analysis 63

B DOA Results 69

P148620.PDF [Page: 8 of 89]

List of Figures

1 Configuration for the data measurements. 11

2 The routes for the mobile transmitter. 12

3 A typical I channel signal. 15

4 Q channel signal generated by applying the Hilbert transform to the I channel signal. 15

5 Power spectrum of the complex signal. 16

6 A typical amplitude distribution of the calibration function. 20

7 A typical phase distribution of the calibration function. 20

8 A typical amplitude distribution after calibration. 21

9 A typical phase distribution after calibration. 21

10 Typical real components of the near-field multipath signals; — channel 1; -.- channel 2. 25

11 Typical imaginary components of the near-field multipath signals; — channel 1; -.- channel 2. 25

12 A typical temporal auto-correlation function of the near-field multipath signal. 26

13 A typical power spectrum of the near-field multipath signal. 26

14 Typical cross-correlation coefficients of the near-field multipath signals. . . . 27

15 A typical temporal auto-correlation function of the far-field multipath signal. 27

16 A typical power spectrum of the far-field multipath signal. 28

17 Typical cross-correlation coefficients of the far-field multipath signals. 28

18 DOA mean square errors versus SNR. 37

19 DOA mean square errors versus SNR (an enlarged section for Fig. 18). . . . 37

20 A typical 2D-DFT result (one source). 41

P148620.PDF [Page: 9 of 89]

21 DFT patterns (one source). 42

22 DFT patterns (one source). 43

23 Typical spatial spectra derived using the MUSIC algorithm. 44

24 A typical 2-D spatial spectrum derived using the spatio-temporal approach. . 45

25 A typical spatial spectrum derived using the two-step FBLP algorithm, DOA=11.3deg. 48

26 The scattered plot for DOA estimates derived using the 2-D DFT technique. 48

27 The scattered plot for DOA estimates derived using the MUSIC algorithm. . 49

28 The scattered plot for DOA estimates derived using the spatio-temporal algorithm. 49

29 The scattered plot for DOA estimates derived using the two-step FBLP algorithm. 50

30 MSE versus signal power level. 50

31 The 2-D DFT DOA results for Case 1. 54

32 The MUSIC DOA results for Case 1. 54

33 The DOA results derived usin the spatio-temporal method for Case 1. 55

34 The 2-D DFT DOA results for Case 2. 55

35 The MUSIC DOA results for Case 2. 56

36 The DOA results derived usin the spatio-temporal method for Case 2. . . . 56

37 The 2-D DFT DOA results for Case 3. 57

38 The MUSIC DOA results for Case 3. 57

39 The DOA results derived usin the spatio-temporal method for Case 3. 58

40 The 2-D DFT DOA results for Case 4. 58

41 The MUSIC DOA results for Case 4. 59

42 The DOA results derived usin the spatio-temporal method for Case 4. 59

P148620.PDF [Page: 10 of 89]

43 Temporal auto-correlation function of the near-field multipath signal. 64
44 Power spectrum of the near-field multipath multipath signals. 64
45 Cross-correlation coefficients of the near-field multipath signals. 65
46 Temporal auto-correlation function of the near-field multipath signal. 65
47 Power spectrum of the near-field multipath multipath signals. 66
48 Cross-correlation coefficients of the near-field multipath signals. 66
49 Temporal auto-correlation function of the far-field multipath signal. 67
50 Power spectrum of the far-field multipath multipath signals. 67
51 Cross-correlation coefficients of the far-field multipath signals. 68
52 The 2-D DFT DOA estimates for a-files (Mar. 1993). 70
53 The MUSIC DOA estimates for a-files (Mar. 1993). 70
54 The spatio-temporal DOA estimates for a-files (Mar. 1993). 71
55 The 2-D DFT DOA estimates for b-files (Mar. 1993). 71
56 The MUSIC DOA estimates for b-files (Mar. 1993). 72
57 The spatio-temporal DOA estimates for b-files (Mar. 1993). 72
58 The two-step FBLP DOA estimates for b-files (Mar. 1993). 73
59 The 2-D DFT DOA estimates for h-files (Mar. 1993). 73
60 The MUSIC DOA estimates for h-files (Mar. 1993). 74
61 The spatio-temporal DOA estimates for h-files (Mar. 1993). 74
62 The two-step FBLP DOA estimates for h-files (Mar. 1993). 75
63 The 2-D DFT DOA estimates for i-files (Mar. 1993). 75
64 The MUSIC DOA estimates for i-files (Mar. 1993). 76
65 The spatio-temporal DOA estimates for i-files (Mar. 1993). 76
66 The two-step FBLP DOA estimates for i-files (Mar. 1993). 77

P148620.PDF [Page: 11 of 89]

67 The 2-D DFT DOA estimates for j-files (Mar. 1993). 77

68 The MUSIC DOA estimates for j-files (Mar. 1993). 78

69 The spatio-temporal DOA estimates for j-files (Mar. 1993). 78

70 The two-step FBLP DOA estimates for j-files (Mar. 1993). 79

71 The 2-D DFT DOA estimates for n-files (Mar. 1993). 79

72 The MUSIC DOA estimates for n-files (Mar. 1993). 80

73 The spatio-temporal DOA estimates for n-files (Mar. 1993). 80

74 The two-step FBLP DOA estimates for n-files (Mar. 1993). 81

1 Introduction

Modern spectrum estimation techniques have been used to improve the performance of direction finding (DF) systems in terms of accuracy and resolvability. However, there still exists a significant source of error that limits the accuracy in DF. When a DF system operates in a multipath environment, its performance is degraded to a certain degree. It is commonly believed that the reason why the accuracy of DF systems has not been improved appreciably over the last twenty years or so is the lack of understanding of the effects of multipath. Therefore, Defence Research Establishment Ottawa (DREO), in conjunction with Communication Research Laboratory (CRL) at McMaster University, has been carried out a series of research activities to study the multipath effects on a DF system and to investigate the techniques to deal with these effects.

As part of the ongoing research, the objective of the present project has been to establish a real DF database and to carry out a comprehensive analysis of the data. To achieve this goal, an experimental eight channel DF system, developed at DREO, was used to carry out data measurement in a series of trials. The receiving array consists of eight sensors , each of which consists of a dipole antenna element and a receiver. The transmitters are used to simulate a complex signal environment and can be operated in a continuum of frequencies in the VHF band. Based on the collected data, we have carried out the development of an appropriate signal model and studied the characteristics of multipath signals. Furthermore, we have investigated

a number of direction-of-arrival algorithms and evaluated their performance based on the real data. In this report, we provide a description and give results, where appropriate, for the following major activities:

1. experimental trials
2. signal modelling
3. data calibration
4. analysis of characteristics
5. development and investigation of practical techniques for direction finding
6. analysis results

P148620.PDF [Page: 14 of 89]

2 Measurements

Measurements were conducted during Nov. 1992 and Mar. 1993. There were basically three types of measurements: (1) one-source measurements, (2) two-source measurements, (3) mobile source measurements.

2.1 The Measurement System

The measurement system is experimental eight-channel DF system developed at DREO [1]. The receiving array consists of eight sensors , each of which consists of a dipole antenna element and a receiver. The receiver consists of the RF, IF, and data acquisition subsystems. The RF frequency for the trials was in the range of 60 MHz. The baseband signals were sampled at 1 kHz. For more details about the system, one is referred to [1].

2.2 One-Source Measurements

In Fig. 1 the setup for the experimental trials is shown. For one-source measurements, only Transmitter 1 (Tx 1 in Fig. 1) was in operation. Seventeen pre-determined locations arranged in a straight line parallel to the array axis were designated to be the transmitter positions. The spacing of these positions was 3.05 m. Data was collected for each between these positions.

P148620.PDF [Page: 15 of 89]

2.3 Two Source Measurements

For two-source measurements, both Transmitters 1 and 2 (Tx 1 and Tx 2 in Fig. 1) were in operation. Data was collected for different positions of Transmitter 1 while the position of Transmitter 2 was left fixed. Data was also collected for different power levels of Transmitter 1 while both the transmitters were left fixed.

2.4 Mobile Source Measurements

For mobile source measurements, Transmitter 2 was mounted on an automobile. Transmitter 1 was also in operation and fixed at the boresight of the array. The automobile was driven on roads in the vicinity of the experimental site (Fig. 2). Data was collected while the automobile was stationary. Once the measurement was taken, the automobile was then moved to next position and stopped for the next measurement. The positions of the automobile were determined based on the distance by which it had travelled with respect to a reference point. The corresponding angular positions were then determined with the assistance of a map of the area.

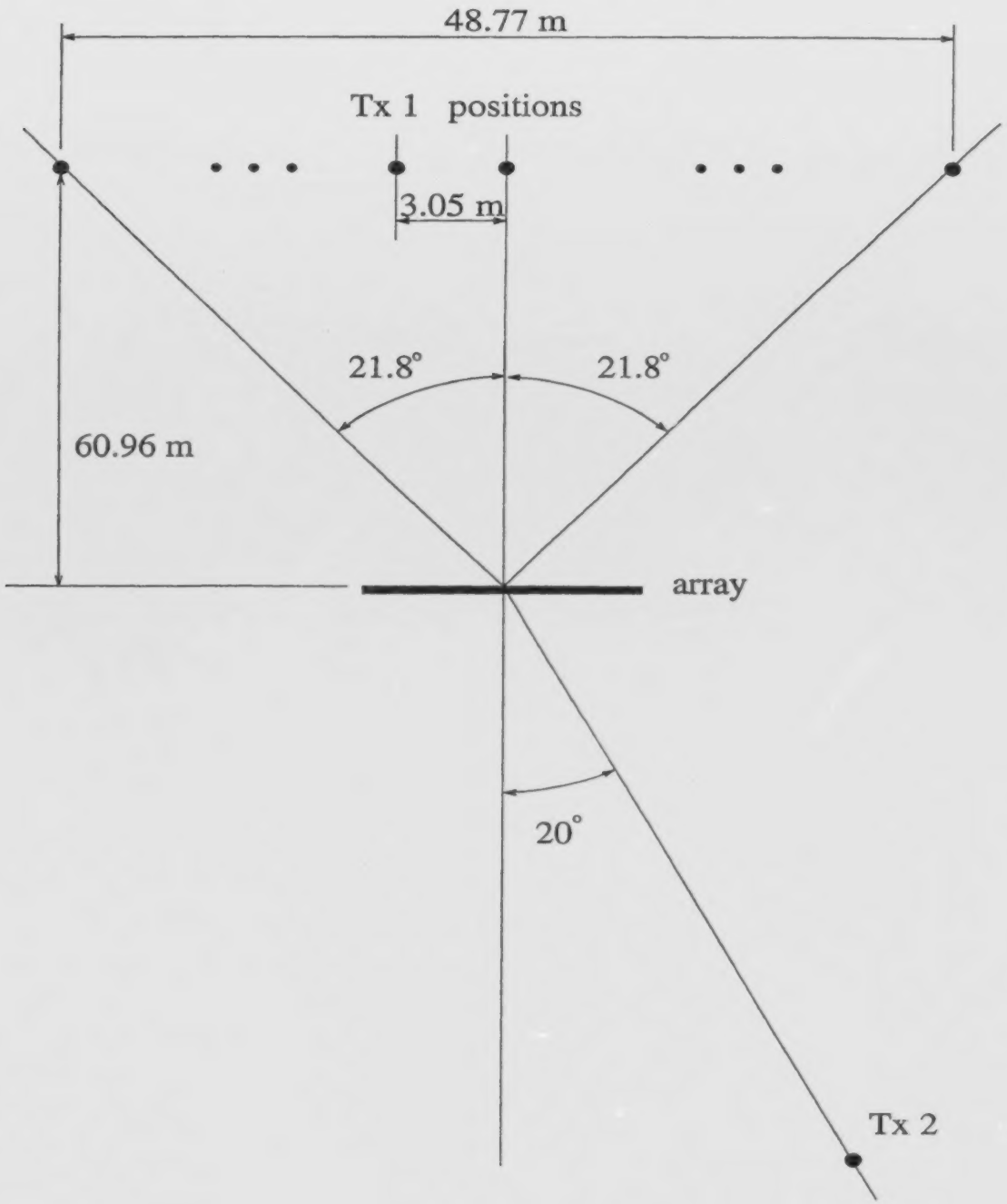

Figure 1: Configuration for the data measurements.

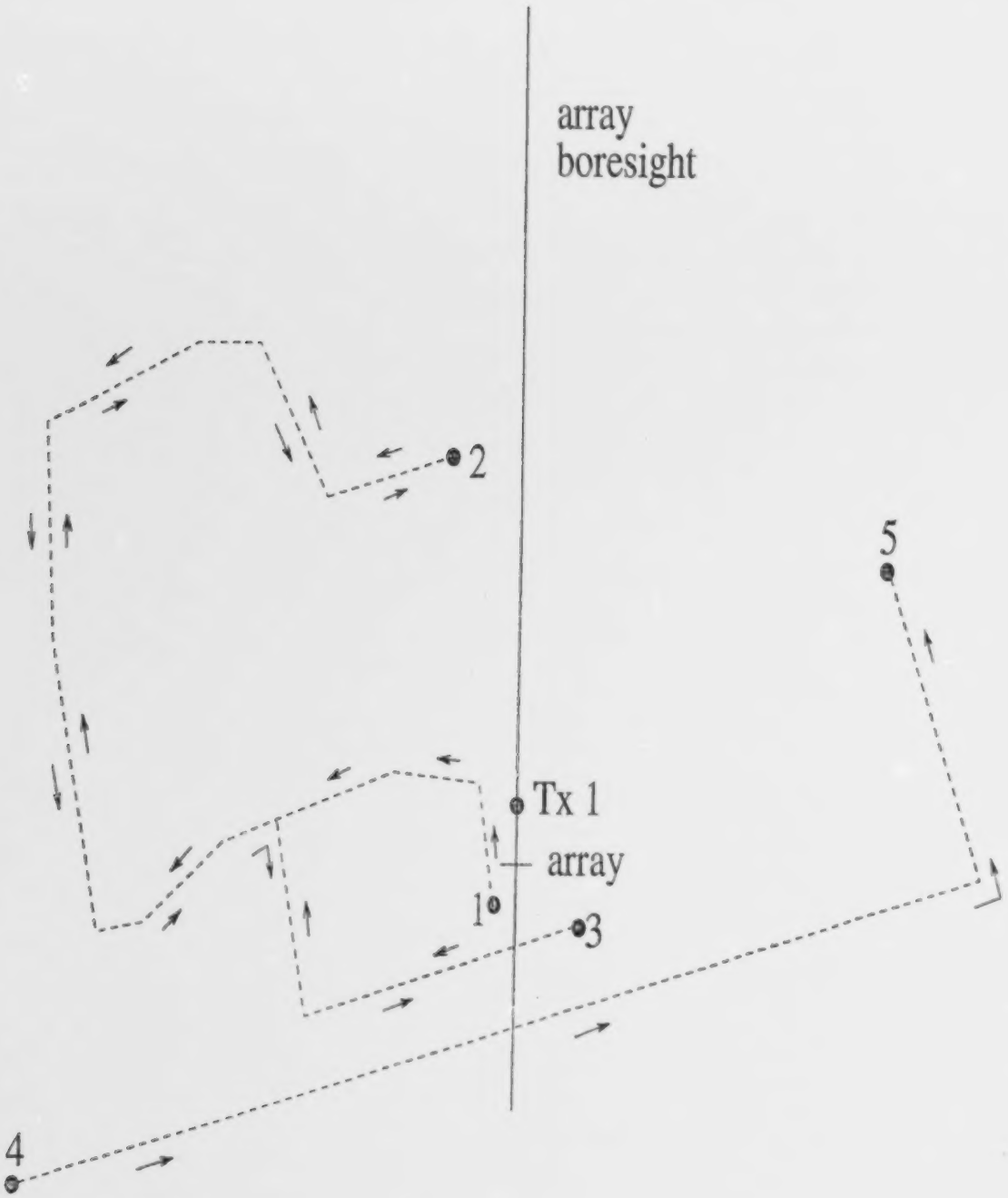

Figure 2: The routes for the mobile transmitter.

P148620.PDF [Page: 18 of 89]

3 Signal Modelling

Usually in the DF system, both the in-phase (I) channel and quadrature (Q) channel are required to form the complex signal. In practice, it is usually found that an imbalance between the I-channel and the Q-channel exists, i.e. the phase between the I- and Q- channels is not exactly 90 degree out of phase. This departure from orthogonality reduces the DF accuracy of the target estimates. Devising a technique for compensating for the imbalance is usually difficult. This difficulty is avoided by generating the Q-channel component from the I-channel component. The cost is the loss of real quadrature information. The Q-channel component is generated from I-channel component using the digital Hilbert transform. The Hilbert transform frequency response is:

$$H(e^{j\omega}) = -jsign(\omega) \tag{1}$$

The complex (analytic) signal representation of received signal can be expressed as

$$X(t) = x(t) + j\widetilde{x(t)} \tag{2}$$

where the tilde denotes the Hilbert transform operator. The above expression is the signal model used to carry out data analysis and algorithm evaluation. The real $x(t)$ usually takes the form of

$$x(t) = A(t)cos(\omega_I t + \psi) \tag{3}$$

where A(t) is the complex amplitude which can be expressed as

$$A(t) = \sum_{n=-N}^{N} A_n e^{j\omega nt}, \tag{4}$$

where ω_I is intermediate angular frequency, and ψ is initial phase. Expressing $x(t)$ in an exponential form, we obtained

$$x(t) = \sum_{n=-N}^{N} \frac{A_n}{2}(e^{j[(\omega_I+\omega n)t+\psi]} + e^{-j[(\omega_I-\omega n)t+\psi]}) \tag{5}$$

where $\omega = \frac{2\pi}{T}$ and T is observation time. Through simple mathematical manipulation, the analytic form of $x(t)$ (i.e. the complex signal) is

$$X(t) = \sum_{n=-N}^{N} A_n e^{j[(\omega_I+\omega n)t+\psi]} \tag{6}$$

In Fig. 3 is shown the I channel component and in Fig. 4 the Q channel component which was generated by applying the Hilbert transform to the I channel signal. In Fig. 5 is given the spectrum of the complex signal $X(t)$. It should be noted that the above the Hilbert transform is an ideal one in that the impulse response is infinite and non-causal. Since the data is processed in an off-line manner, the non-causality does not cause any problem. The finite length of data may present problems. However, since the data length is relatively long (2000 points), the leakage due to finite data length is very small, as shown in Fig. 5.

P148620.PDF [Page: 20 of 89]

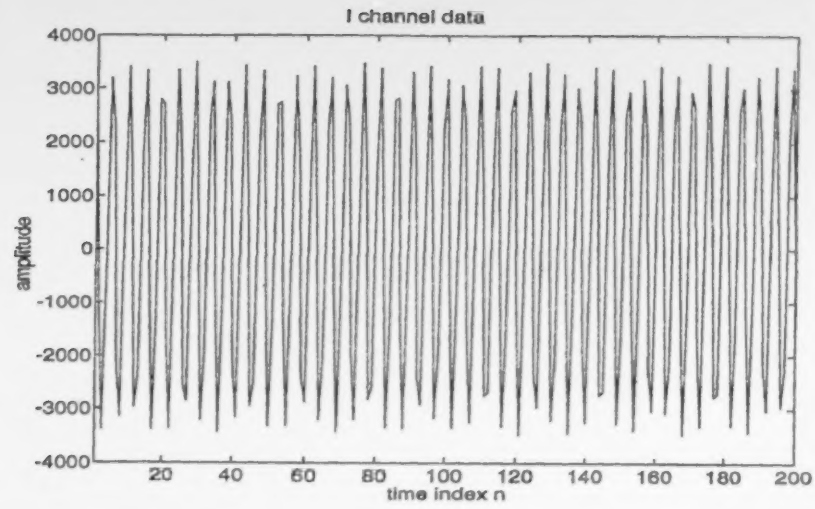

Figure 3: A typical I channel signal.

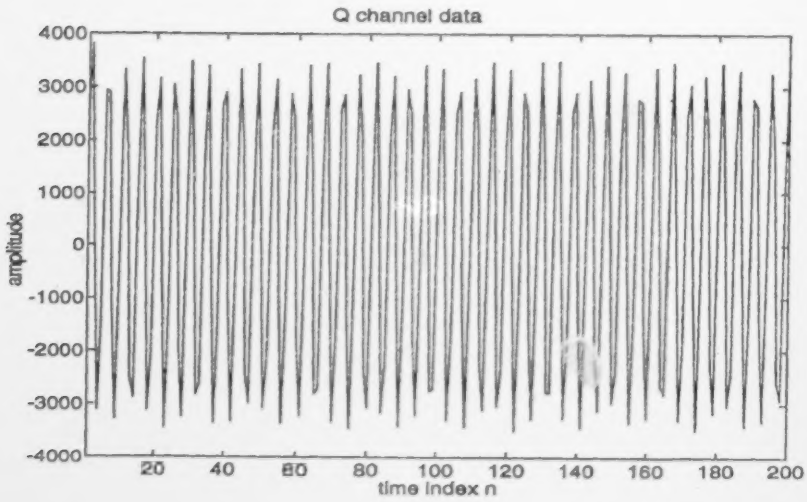

Figure 4: Q channel signal generated by applying the Hilbert transform to the I channel signal.

P148620.PDF [Page: 21 of 89]

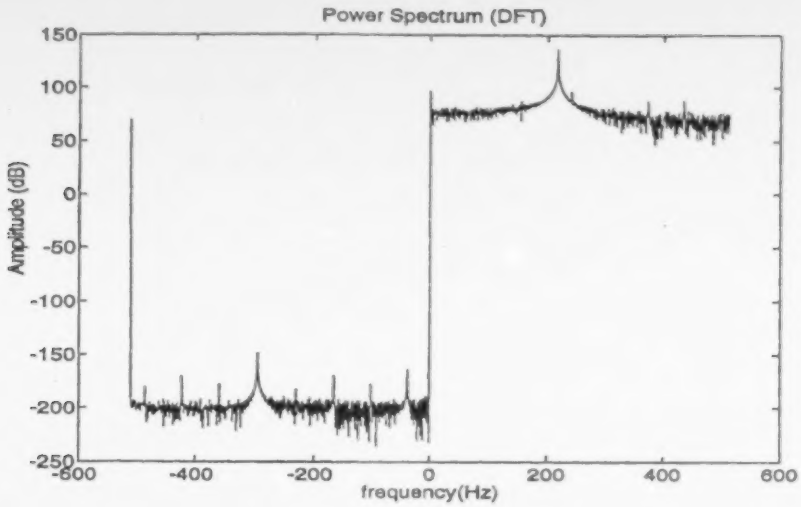

Figure 5: Power spectrum of the complex signal.

P148620.PDF [Page: 22 of 89]

4 Data Calibration

The experimental antenna array consists of eight dipole antennas, for each of which there is an independent receiver. Since the gain and phase of each receiver are different from the others, data calibration is required to correct the gain and phase difference. Although there are a number of methods for carrying out data calibration, we have chosen a simple but practical technique for data calibration, where the effect due to the signal environment is implicitly considered.

In order to find the calibration error function, a known source is required with the steering direction vector expressed as

$$q = [1 \; e^{j\phi} \; ... \; e^{j7\phi}]^T \tag{7}$$

where ϕ is related to the spatial frequency $\phi = \frac{2\pi}{\lambda} d \sin\theta$, λ is the wavelength of the carrier wave, d is the element spacing, θ is the direction of arrival(DOA), and T denotes transpose operator.

The signal received by the sensors from a known source can be expressed in a vector form, i.e.

$$x = Ae^{j\psi} \cdot q \tag{8}$$

where ψ is a random phase and A is the signal amplitude. The complex gains of the eight receivers can be expressed in vector form as

$$G = [G_1 e^{j\phi_1} \; ... \; G_8 e^{j\phi_8}]^T. \tag{9}$$

It follows that the outputs of the eight channels are

$$X_0 = [AG_1 e^{j\psi + j\phi_1} \; AG_2 e^{j\psi + j\phi_2 + j\phi} \; ... \; AG_8 e^{j\psi + j\phi_8 + j7\phi}]^T \tag{10}$$

P148620.PDF [Page: 23 of 89]

The calibration error function is obtained by normalizing X_0 by $qAG_1e^{j\phi_1+j\psi}$, i.e.

$$X_1 = [1 \ \frac{G_2}{G_1}e^{j\phi_2-j\phi_1} \ ... \ \frac{G_8}{G_1}e^{j\phi_8-j\phi_1}]^T. \tag{11}$$

Since the received signals are contaminated by background noise, statistical mean values are used as the estimate of the calibration error function. The background noise is assumed to be additive white Gaussian noise. The estimates of $AG_ie^{j\phi_i+j\psi}$ is given by

$$\tilde{g}_i = \frac{1}{N}\sum_{n=1}^{N} AG_i(n)e^{j\phi_i(n)+j\psi} \tag{12}$$

where N is the number of time samples for the temporal average. In our case, N was taken to be 2048. The estimate of the calibration function is given as

$$\tilde{X}_1 = [1, \frac{\tilde{g}_2}{\tilde{g}_1}, ..., \frac{\tilde{g}_8}{\tilde{g}_1}]^T. \tag{13}$$

In Fig. 6 the amplitude distribution of a typical calibration function is shown and in Fig. 7 the corresponding phase is shown. Shown in Figs. 8 and 9 is an example of the averaged amplitude and phase distributions of a set of calibrated data for the case of one incoming signal. For perfect calibration, the amplitude of each channel will be the same and the phase difference between two adjacent channels will also be the same. However, it can be observed that there are residual errors after calibration, that is, the amplitude distribution is not perfectly uniform and the phase is not perfectly linear. This small amount of residual error will cause errors in the DOA estimates in the subsequent analysis. The residual errors may be due to (1) motion of the antenna elements, (2) uneven spacing between the

antenna elements, (3) and other random errors such as those in quatization.

P148620.PDF [Page: 25 of 89]

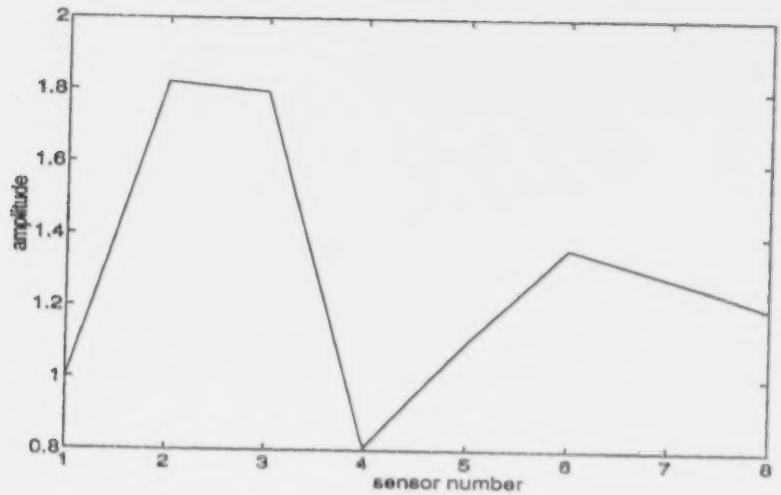

Figure 6: A typical amplitude distribution of the calibration function.

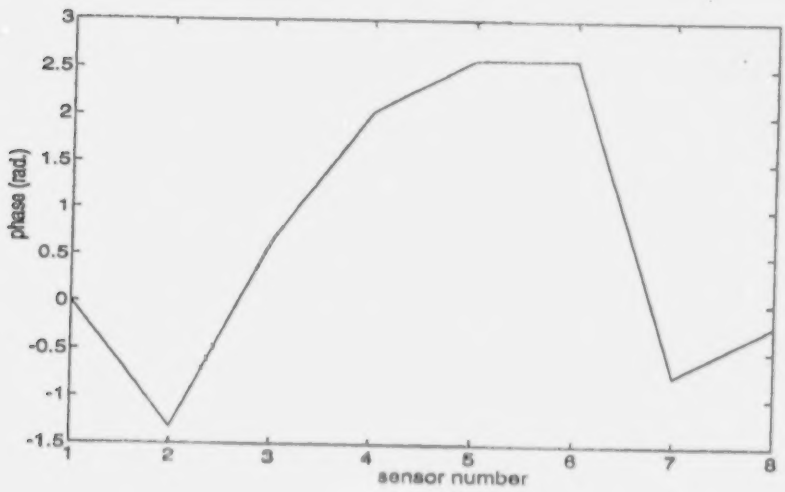

Figure 7: A typical phase distribution of the calibration function.

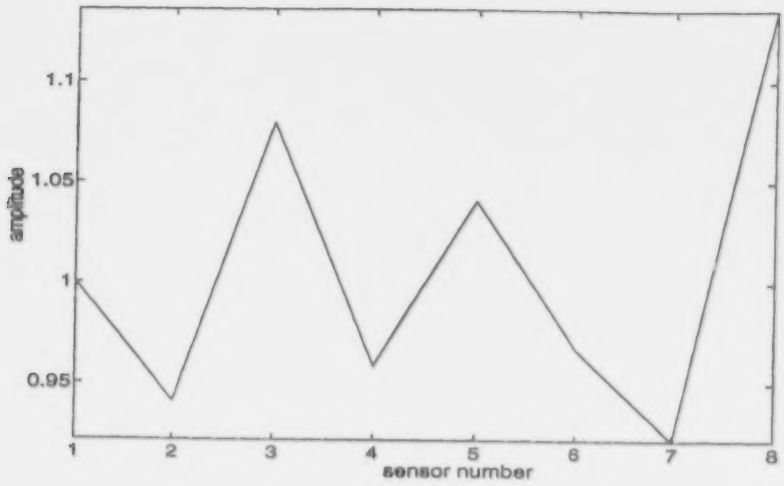

Figure 8: A typical amplitude distribution after calibration.

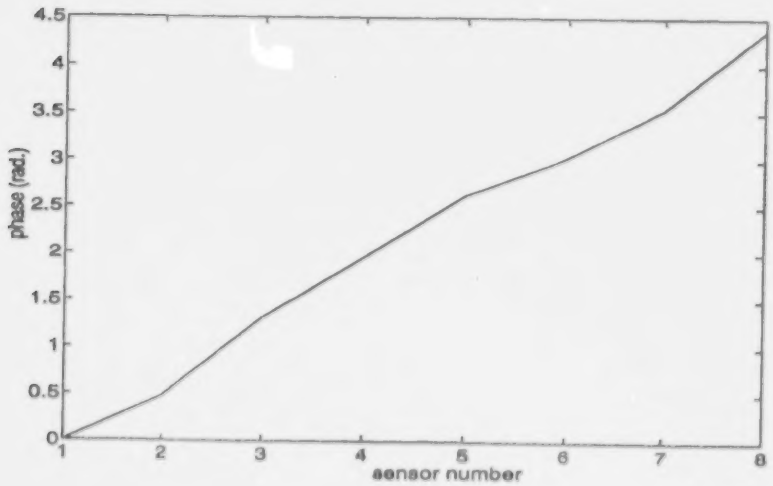

Figure 9: A typical phase distribution after calibration.

P148620.PDF [Page: 27 of 89]

5 Analysis of Signal Characteristics

In a multipath environment, the received signal consists of direct path component and components reflected from the surface. In a practical system, there are additional error sources such as those caused by the phase error in the local oscillator and the vibrations of the antenna elements. These additional errors are in the form of multiplicative errors. For the case of one source, the overall received signal can be expressed as

$$x(t) = [x_d(t) + x_m(t)]x_a(t) + \varepsilon(t) \tag{14}$$

where $x_d(t)$ represents the direct component with a constant amplitude, $x_m(t)$ represents the multipath components, $x_a(t)$ represents the additional errors, and $\varepsilon(t)$ represents the receiver noise which is assumed to be white Gaussian noise. Expressing $x(t)$ in a polar form, we have

$$x(t) = A(t)e^{j(\omega_c t + \phi(t))} + \varepsilon(t) \tag{15}$$

where ω_c is carrier frequency. Assuming that the $A(t)e^{j\phi(t)}$ can be expressed using Fourier coefficients,

$$A(t)e^{j\phi(t)} = \sum_{n=-N}^{N} A_n e^{j\omega_n t} \tag{16}$$

where ω_n is determined by observation period and A_n are the Fourier coefficients, we can express (15) as

$$x(t) = \sum_{n=-N}^{N} A_n e^{j(\omega_c + \omega_n)t} + \varepsilon(t) \tag{17}$$

Removing the carrier frequency (the direct signal), we obtain baseband signal

$$m(t) = \sum_{n=-N}^{N} A_n e^{j\omega_n t} + \varepsilon(t) \tag{18}$$

Fig. 10 shows the real components of a typical signal $m(t)$ from Channels 1 and 2. Fig. 11 shows the corresponding imaginary components. The Fourier coefficients A_n of $m(t)$ are given by the Fourier transform of $m(t)$,

$$A_n = \sum_{k=-N}^{N} m(k) e^{-j\omega_n k}. \tag{19}$$

The temporal characteristics of $m(t)$ can be observed from the normalized autocorrelation function of $m(t)$, which is given as

$$R(\tau) = \frac{1}{R(0)} \sum_{k=1}^{N} m(k)m(k-\tau), \quad for\ \tau = 1, ..., N \tag{20}$$

where

$$R(0) = \sum_{k=1}^{N} m(k)m(k). \tag{21}$$

Furthermore, the spatial characteristics of $m(t)$ can be derived from the cross-correlation coefficients $R_{ij}(0)$ between the signal of the i^{th} channel, $m_i(t)$, and that of the j^{th} channel, $m_j(t)$,

$$R_{ij}(0) = \sum_{k=1}^{N} m_i(k)m_j(k). \tag{22}$$

In the following examples, two typical cases are presented. The first case is based on a data set for which there is only one signal present at the near field. Figs. 12, 13, and 14 show the normalized autocorrelation function, the corresponding spectrum, and the cross-correlation coefficients, respectively. In the second case, the results are based on another data set for

P148620.PDF [Page: 29 of 89]

which there is only one signal present in the far field. Figs. 15, 16, and 17 show the normalized autocorrelation function, the corresponding spectrum, and the cross-correlation coefficients, respectively. By comparing the two cases, obvious differences can be observed. In the near-field case, there are relatively strong temporal and spatial correlations. As well, significant peaks are observed at low frequencies in the spectrum. In the far field case, the correlations are lower and there is no significant peak in the spectrum. Additional data sets have been analyzed and as shown in Appendix. The results show that the spectrum is spread from $\pm 4Hz$ to $\pm 6Hz$ and there are high temporal and spatial correlations in the near-field cases. In contrast, for the far field cases, these characteristics become much less noticeable and significant. It is apparent that the errors (including multipath, phase errors, and antenna vibrations) are stronger and more influential for near-field than for far field.

P148620.PDF [Page: 30 of 89]

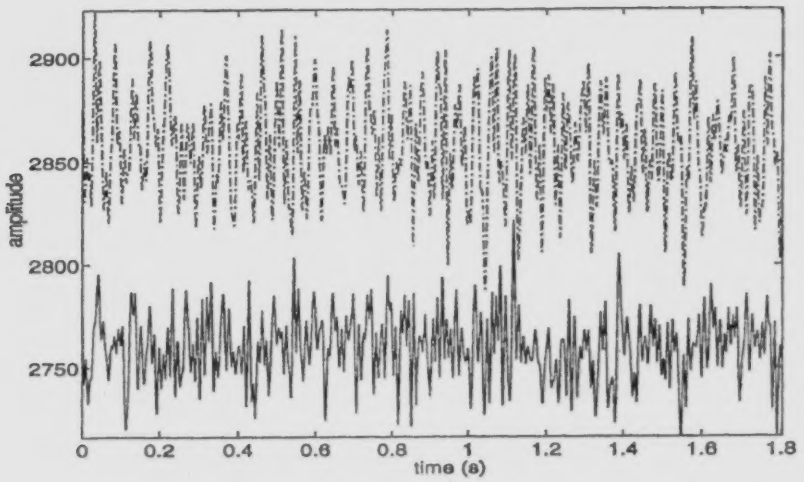

Figure 10: Typical real components of the near-field multipath signals; — channel 1; -.- channel 2.

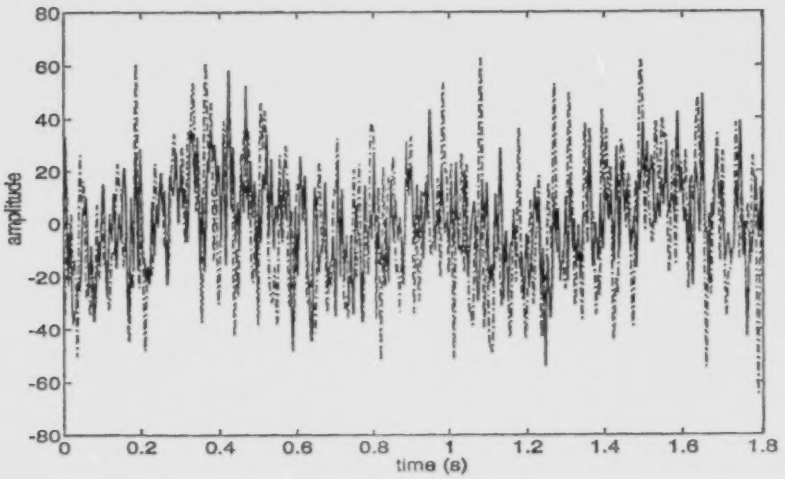

Figure 11: Typical imaginary components of the near-field multipath signals; — channel 1; -.- channel 2.

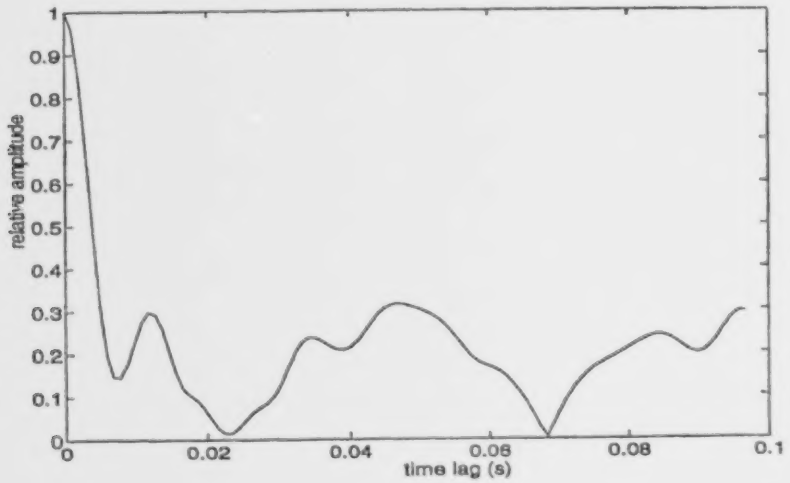

Figure 12: A typical temporal auto-correlation function of the near-field multipath signal.

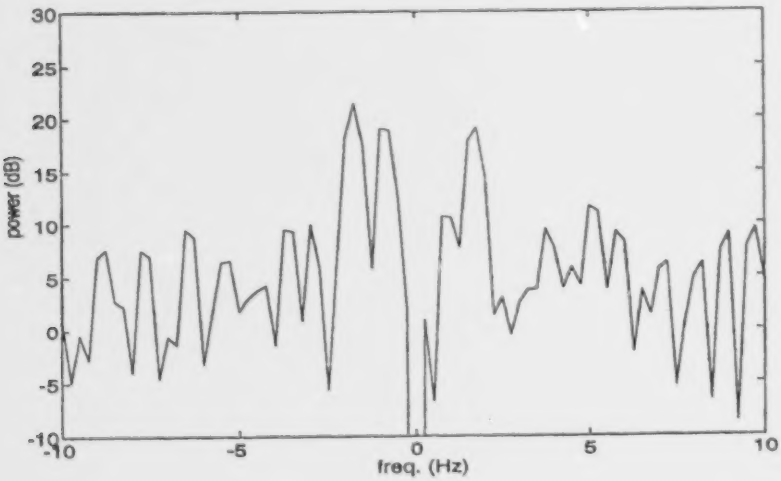

Figure 13: A typical power spectrum of the near-field multipath signal.

P148620.PDF [Page: 32 of 89]

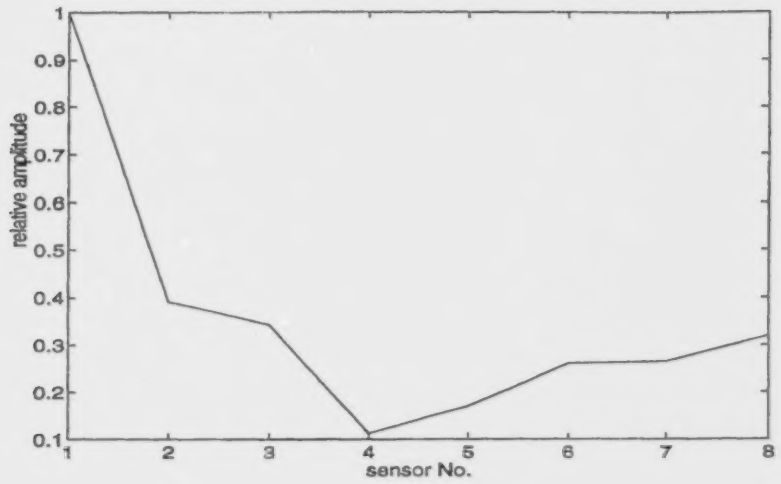

Figure 14: Typical cross-correlation coefficients of the near-field multipath signals.

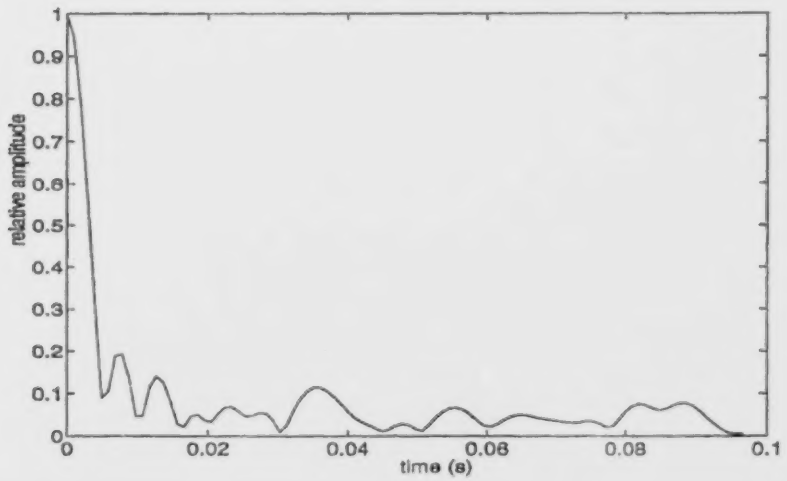

Figure 15: A typical temporal auto-correlation function of the far-field multipath signal.

P148620.PDF [Page: 33 of 89]

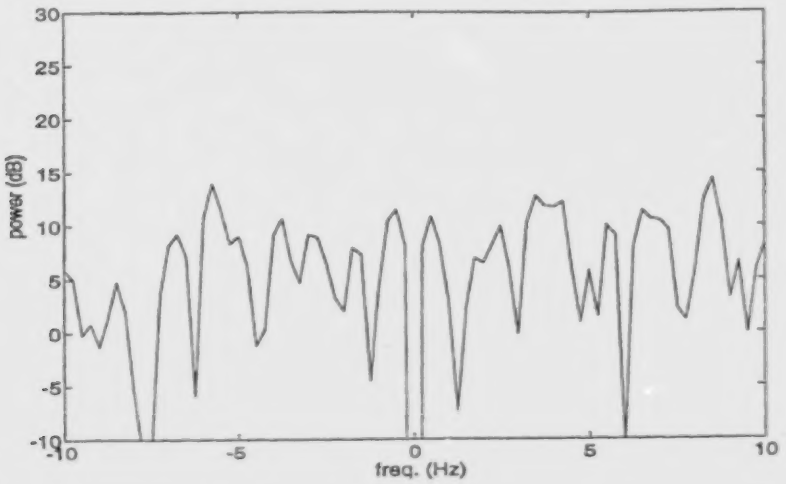

Figure 16: A typical power spectrum of the far-field multipath signal.

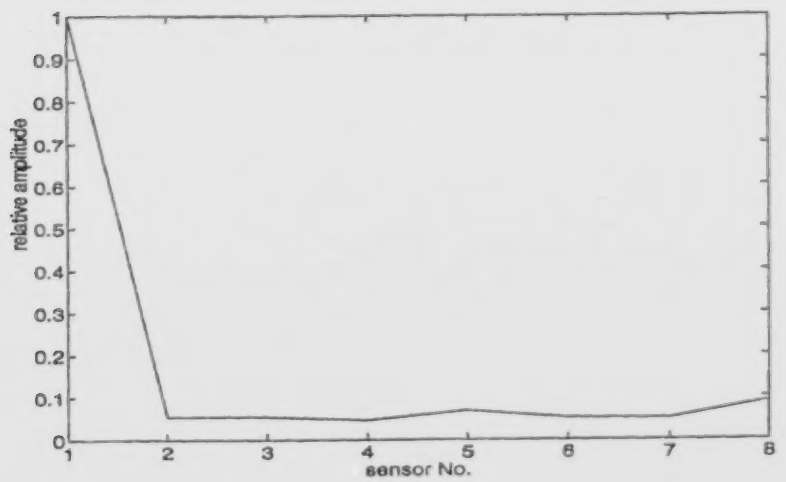

Figure 17: Typical cross-correlation coefficients of the far-field multipath signals.

P148620.PDF [Page: 34 of 89]

6 DF Algorithms

6.1 DFT

In the investigation of the performance of direction finding methods , the discrete Fourier transform (DFT) is used as a benchmark for other methods. In our case, the 2-D DFT is used to obtain both the angle-of-arrival and signal frequency (baseband) information. The 2-D DFT can be expressed as

$$X(k,l) = \sum_{n=1}^{N-1} \sum_{m=1}^{M-1} x(n,m) W_N^{kn} W_M^{lm} \quad for \begin{cases} k = 1, ..., N \\ l = 1, ..., M \end{cases} \tag{23}$$

where $W_N = e^{-j\frac{2\pi}{N}}$, $x(n,m)$ is two dimensional spatio-temporal signal, k is the temporal frequency index, and l is the spatial frequency index. The computation of $X(k,l)$ is carried out using the vector-radix fast Fourier transform. The resolution is $\frac{2\pi}{N}$ (digital frequency).

6.2 MUSIC

The MUSIC algorithm [2] is a high-resolution technique which is able to resolve signals that are spaced less than an antenna beamwidth. The approach is summarized as follows. Assuming that there are K narrowband incidental waves impinging on the DF array from sources in the far field, we can express the $N \times 1$ received signal vector $\mathbf{x}$ as

$$\mathbf{x} = S\mathbf{a} + \mathbf{n}, \tag{24}$$

where $\mathbf{a}$ is a $K \times 1$ signal amplitude vector, $\mathbf{n}$ is an N-dimensional noise vector, and S is $N \times K$ direction matrix. The noise vector $\mathbf{n}$ is assumed to

be complex Gaussian distributed with zero mean. Its covariance matrix is given by $\sigma^2 I$, where σ^2 is an unknown scalar and I is an $N \times N$ identity matrix. The noise components are considered to be uncorrelated with the signals. In addition, each column of the matrix S corresponds to particular direction of arrival. It is assumed that the K direction vectors in S are linear independent of each other. It is required that the number of incident waves is known and the number of sensors is greater than that the number of incoming signals.

Based on the above assumptions, the covariance matrix of the received signal $\mathbf{x}$ can be expressed as

$$R_x = SR_aS + \sigma^2 I \tag{25}$$

where $R_a = E[\mathbf{a}\mathbf{a}^H]$ is the source signal covariance matrix and H denotes the Hermitian transpose. If there is no correlation between the incident waves, the source signal covariance matrix will have a rank of K.

The covariance matrix R_x can be diagonalized by a nonsingular orthogonal matrix which contains all the eigenvectors of R_x. The resultant diagonal matrix contains the associated engenvalues. Asymptotically, the number of eigenvalues that are greater than the noise power corresponds to the number of signals. These eigenvalues are usually referred to as the principal eigenvalues. The corresponding eigenvectors span a subspace called the signal subspace E_s. The rest of the eigenvectors are contributed by the noise and therefore they span the noise subspace E_n. The noise subspace

P148620.PDF [Page: 36 of 89]

has the following property,

$$S \perp span(E_n), \tag{26}$$

that is $S^H E_n = \mathbf{0}$. Hence , the peaks of the following function

$$P(\theta) = \frac{1}{\mathbf{s}^H E_n E_n^H \mathbf{s}} \tag{27}$$

indicate the estimated DOA, where s is in the continuum of steering direction vector.

6.3 Spatio-temporal Estimation

The main motivation for using this algorithm is that in addition to the spatial information, the temporal information can be used to improve the accuracy in DF estimates in a multipath environment.

The spatio-temporal estimation algorithm is given as follows. For a receiving array comprised of N sensors, the N received signals $x_1(t), x_2(t), ..., x_N(t)$ can be conveniently expressed as a signal vector

$$X(t) = [x_1(t), x_2(t), ...x_N(t)]^T \tag{28}$$

which consists of signal components $\mathbf{S}(t)$ and the noise component, i.e.

$$X(t) = \mathbf{S}(t) + \mathbf{n}(t) \tag{29}$$

For simplicity we first consider a signal model for one source, which can then be extended to multiple sources. The signal at time n from the i^{th} sensor can be expressed as

$$r_i(n) = \sum_{k=1}^{p} B_k e^{-j\omega_c \tau_i + j\omega_k(n)} + n_i(n) \tag{30}$$

where B_k is signal amplitude related to k^{th} frequency, τ_i is the propagation delay for the signal at the i^{th} sensor with respect to a reference, and n_i is noise term for the i^{th} sensor. For M snapshots, there are $N \times M$ samples, $\{r_i(t+(n-1)T), \quad i=1,...,N, \ n=1,...,M\}$. Grouping the samples to form N $M \times 1$ vectors, we can rewrite (30) in a matrix form

$$R_i(t) = A_i B(t) + \mathbf{n}_i(t), i = 1,...,8 \tag{31}$$

where $R_i(t)$ and $\mathbf{n}_i$ are $M \times 1$ vectors

$$R_i^T(t) = [r_i(t),...,r_i(t+(M-1)T)] \tag{32}$$

$$\mathbf{n}_i^T(t) = [n_i(t),...,n_i(t+(M-1)T)] \tag{33}$$

$B(t)$ is the $p \times 1$ vector,

$$B^T(t) = [B_1,...,B_p] \tag{34}$$

and A_i is $M \times p$ matrix

$$A_i = \begin{bmatrix} e^{-j\omega_c \tau_{i1}} & \dots & e^{-j\omega_c \tau_{i1}} \\ \vdots & \vdots & \vdots \\ e^{-j\omega_c \tau_{i1} + j(M-1)\omega_1 T} & \dots & e^{-j\omega_c \tau_{i1} + j(M-1)\omega_p T} \end{bmatrix} \tag{35}$$

Stacking the $M \times 1$ vectors $\{R_i(t), \ i=1,...,N\}$ to form an $(N \times M) \times 1$ vector $R(t)$, we can simplify the notation and rewrite (31) as

$$R(t) = AB(t) + n(t) \tag{36}$$

where R(t) and n(t) are $(N \times M) \times 1$ vectors:

$$R^T(t) = [R_1^T(t),...,R_N^T(t)] \tag{37}$$

$$n^T(t) = [\mathbf{n}_1^T(t), ..., \mathbf{n}_N^T(t)] \tag{38}$$

and A is $(N \times M) \times p$ matrix

$$A^T = [A_1^T, ..., A_N^T] \tag{39}$$

From (35) it follows that each column of A_i is related to a particular frequency and the direction of arrival. It is easy to extend the one-source signal model to a multiple-source scenario. In the multiple source case, each column of A is associated with a different source DOA and different frequency. We shall denote these column vectors by $a(\theta_i, \omega_j)$, and refer them to as the direction-frequency vectors of sources.

We assume that the noise is zero-mean with variance σ^2 and that it is uncorrelated from sample to sample. We further assume that they are uncorrelated from sensor to sensor and uncorrelated with source signals.

From (36) the correlation matrix of R(t) becomes

$$R_R = E[R(t)R(t)^H] = ASA^H + \sigma^2 I \tag{40}$$

where H is conjugate transpose, I is the identity matrix, and S is the covariance matrix of the sources:

$$S = E[B(t)B^H(t)] \tag{41}$$

In the same manner as described in the previous subsection, we can obtain the signal subspace and noise subspace from the eigenvectors of R_R, which can be used compute the two-dimensional (2-D) spectrum, i.e. the spatio-temporal spectrum. Hence, this method is usually called the spatio-

P148620.PDF [Page: 39 of 89]

temporal method. The noise subspace E is related to A by

$$E \perp span(A), \tag{42}$$

which can be used to determine the DOA and frequency of sources. More specifically, the following function

$$P(\theta, \omega) = \frac{1}{\|a(\theta, \omega)^H E\|^2}$$

will have peaks at $a(\theta_i, \omega_j)$'s which are the steering direction frequency vectors of sources.

6.4 Two-step Prediction Direction Finding

It is known that sinusoidal signals with Gaussian white noise can be expressed using linear prediction model. For example, using outputs of the first six sensors, the output at the seventh sensor can be expressed as

$$x_7 = a_1 x_1 +, ..., a_6 x_6 + e_7 \tag{43}$$

where $a_i's$ are regressive coefficients and e_i's noises. Similarly, the output of the eighth sensor can be written as

$$x_8 = a_1 x_2 +, ..., a_6 x_7 + e_8. \tag{44}$$

substituting (43) into (44), we obtain

$$\begin{aligned} x_8 \;=\; & a_1 a_6 x_1 + (a_1 + a_2 a_6) x_2 + (a_2 + a_3 a_6) x_3 + (a_3 + a_4 a_6) x_4 + \\ & (a_4 + a_5 a_6) x_5 + (a_5 + a_6^2) x_6 + a_6 e_7 + e_8. \end{aligned} \tag{45}$$

For simplicity, we can rewrite (45)

$$x_8 = A_1 x_1 + A_2 x_2 +, ..., + A_6 x_6 + e \tag{46}$$

where

$$A_1 = a_1 a_6$$

$$A_2 = a_1 + a_2 a_6$$

$$A_3 = a_2 + a_3 a_6$$

$$A_3 = a_3 + a_4 a_6$$

$$A_5 = a_4 + a_5 a_6$$

$$A_6 = a_5 + a_6^2$$

$$e = a_6 e_7 + e_8. \tag{47}$$

According to (46), the output of the eighth sensor is predicted using the outputs of the first six sensors. Hence, this method is called the two-step prediction. It requires multiple snapshots to estimate the coefficients A_i. For M snapshots,

$$XA = x_p \tag{48}$$

or

$$\begin{bmatrix} x_{11} & x_{21} & \dots & x_{61} \\ \vdots & \vdots & \vdots & \vdots \\ x_{1M} & x_{2M} & \dots & x_{6M} \\ x_{81}^* & x_{71}^* & \dots & x_{31}^* \\ \vdots & \vdots & \vdots & \vdots \\ x_{8M}^* & x_{7M}^* & \dots & x_{3M}^* \end{bmatrix} \begin{bmatrix} A_1 \\ \vdots \\ A_6 \end{bmatrix} = \begin{bmatrix} x_{81} \\ \vdots \\ x_{8M} \\ x_{11}^* \\ \vdots \\ x_{1M}^* \end{bmatrix} \tag{49}$$

where * stands for conjugate operator. The data matrix X is formed by two matrices. The upper half of X is for forward linear prediction whereas the lower half is for backward linear prediction.

Solving (49) for A in a least square sense and substituting A into (47), we can evaluate the predictor's coefficients, a_i. The angles-of-arrival are indicated by the peaks in the normalized spatial spectrum,

$$P(\omega) = \frac{1}{|1 + \sum_{i=1}^{6} b_i e^{-j\omega i}|^2} \tag{50}$$

where $b_i = -a_{7-i}$, for $i = 1, ..., 6$ and ω is spatial frequency. The performance of this technique is investigated using simulations. For comparison, we carry out the DF simulations using the forward-backward linear prediction, forward-backward two-step prediction, forward linear prediction, and forward two-step prediction methods. The estimation error are computed at different signal-to-noise ratio (SNR) levels and with 200 trials at each SNR level. In Fig. 18 is shown the mean-squared errors versus SNR levels for the four methods. Fig. 19 shows an enlarged section of Fig. 18. It can be observed that the performance of the forward two-step prediction method is better than that of the forward linear prediction method, whereas the forward-backward two-step prediction method is better than that of the forward-backward linear prediction method.

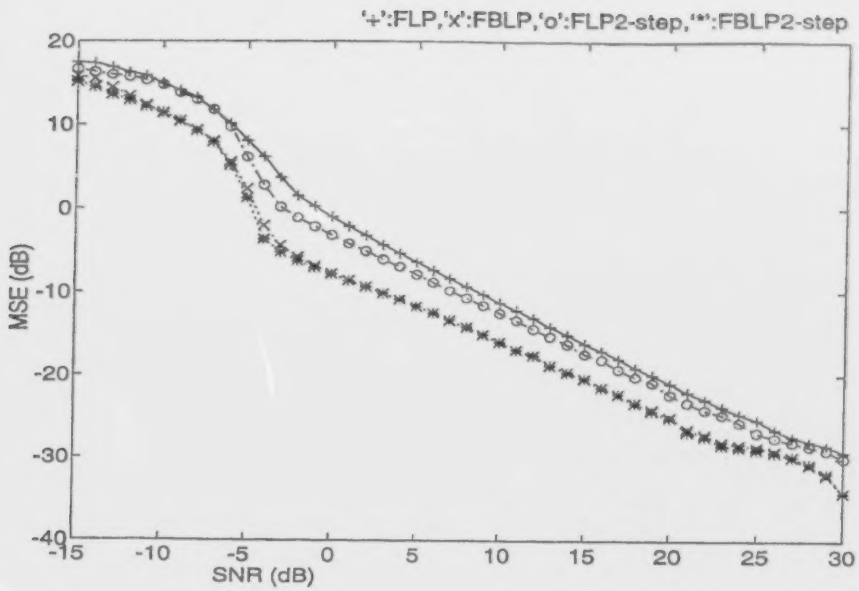

Figure 18: DOA mean square errors versus SNR.

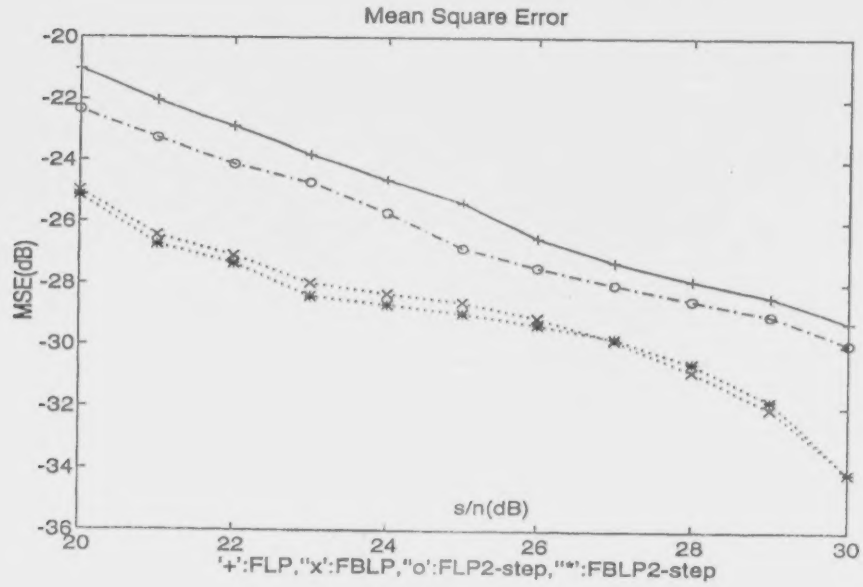

Figure 19: DOA mean square errors versus SNR (an enlarged section for Fig. 18).

7 Analysis Results

Except where indicated, the number of snapshots used for all the analyses is 64. For results derived from DFT, N=1024 and M=64, which implies that the angular resolution is of 0.176° and frequency resolution is of 15.6 Hz. The angular resolution for the peak search in the other three method is 0.1°.

7.1 Typical Results

In the following figures are given a number of representative examples for the methods used in the analysis. In Fig. 20 a typical 2-D DFT result is shown. The maximum point indicates the angle-of-arrival and the signal frequency. In Figs. 21 and 22 are shown the cross-section of the 2-D DFT patterns taken at the frequencies corresponding to the maximum values of the patterns. In these two figures there are 16 small figures which show the cases for different source locations. In each of the small figures are superimposed two sets of results derived from data that was collected at different times (10 minutes apart in average) for the same source location. It can be observed that for each case the two patterns are very consistent with one another. These results suggest that the multipath environment is relatively stationary.

Fig. 23 shows a typical set of results derived using the MUSIC algorithm. It shows the spatial spectrum for different source locations. Again, the results derived from data collected at different times (10 minutes apart

in average) but for the same source locations are superimposed with each other. The consistency between the superimposed patterns supports the suggestion that the multipath environment is relatively stationary.

Fig. 24 shows a typical 2-D spectrum derived using the spatial-temporal technique. The maximum point indicates the angle-of-arrival and the signal frequency.

Fig. 25 is showing a typical spatial spectrum derived using the two-step FBLP technique. The sharp peak indicates the angle-of-arrival.

7.2 Performance Analysis

The performance of a DF algorithm can be evaluated by carrying out computer simulations. However, the signal model used in simulation is usually based on simple assumptions and is not close to realistic situations. In other words, it is very difficult to generate a real-life-like signal environment (multipath, source signal, noise, coupling effect between sensors). Therefore, performance evaluation using real data is indispensable if the characteristics of the DF techniques are to be studied. To evaluate the performance of the DF techniques under different signal strength levels, the following trials were conducted. One source was located at 20° with power level fixed and another source was located at 0°, the power level of which was controllable with a variable attenuator.

At each transmitter power level, data was recorded. The 2-D FFT , MUSIC, spatio-temporal, and forward backward two-step prediction methods were used to process the data. For each power level, 15 sets of 64-snapshot data were analyzed to produce 15 pairs of DOA estimates. Based on the variance of these estimates, the performance was evaluated. In Figs. 26 to 29 the scatter plots of the estimates versus different power levels for the four methods are shown. For the 2-D DFT method, some DOA estimates deviate from the actual source directions (i.e. 0° and 20°) at 0 dB and 10 dB attenuations. The errors were most likely caused by receiver saturation (i.e. nonlinearity) due to a strong source. The DOA estimates for the 0° source begin to deviate considerably from the actual bearing at 30 dB at-

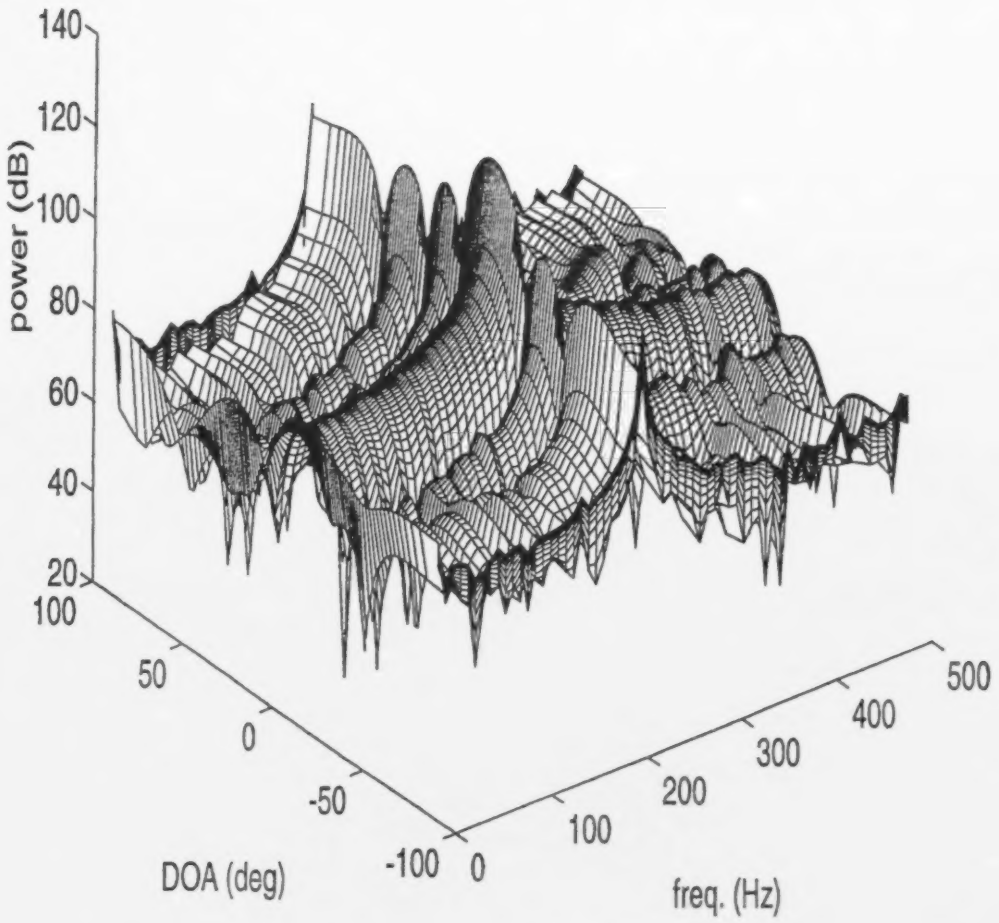

Figure 20: A typical 2D-DFT result (one source).

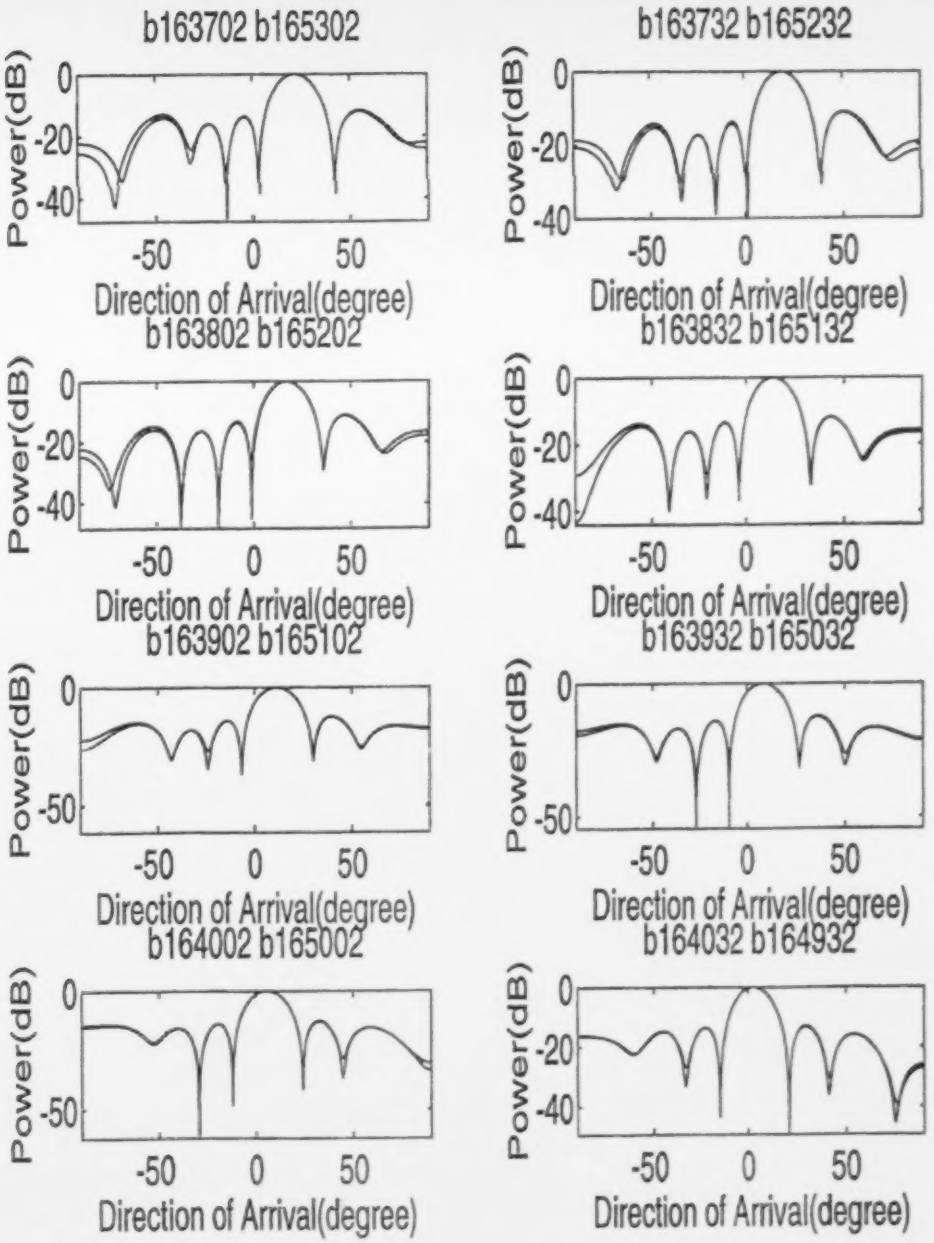

Figure 21: DFT patterns (one source).

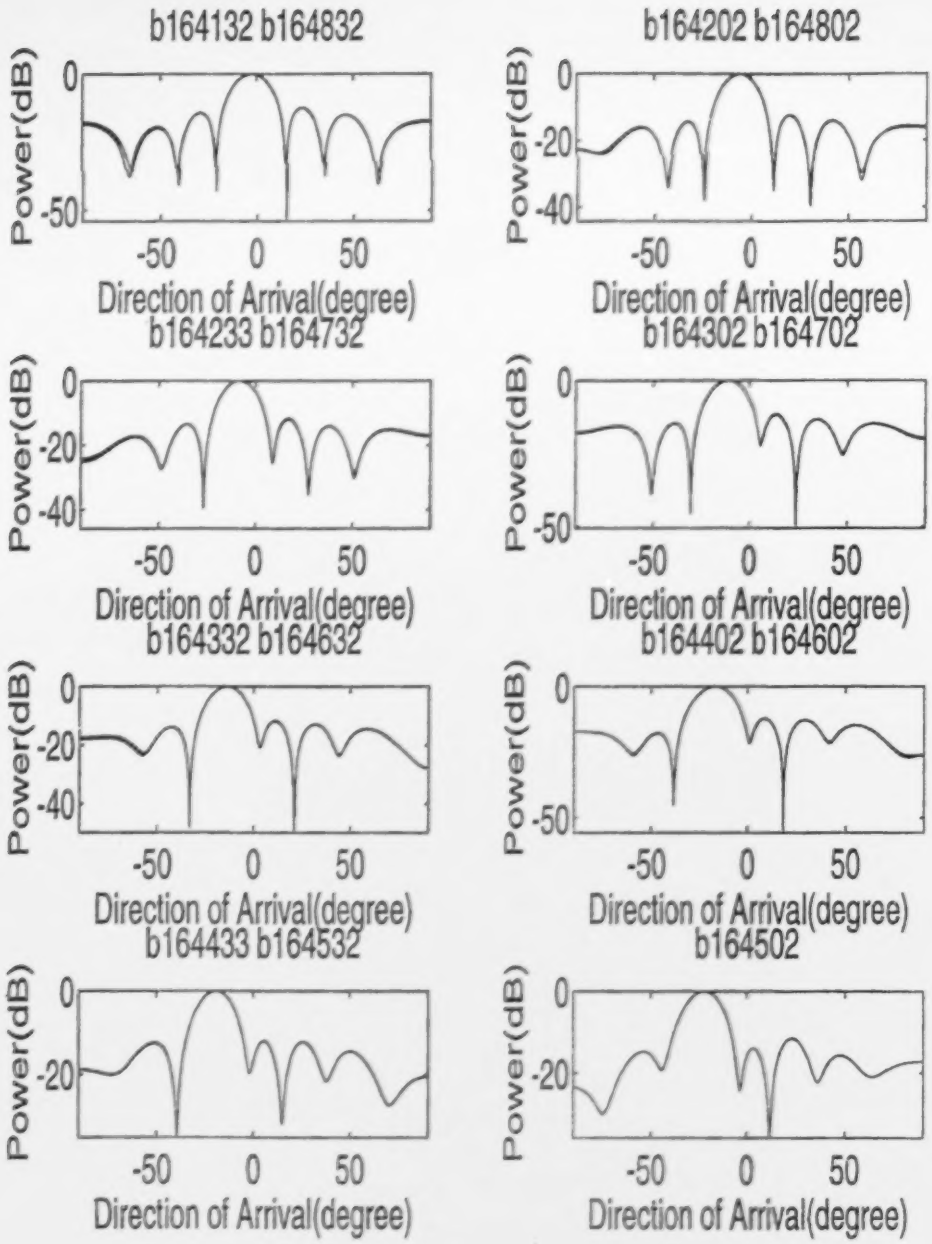

Figure 22: DFT patterns (one source).

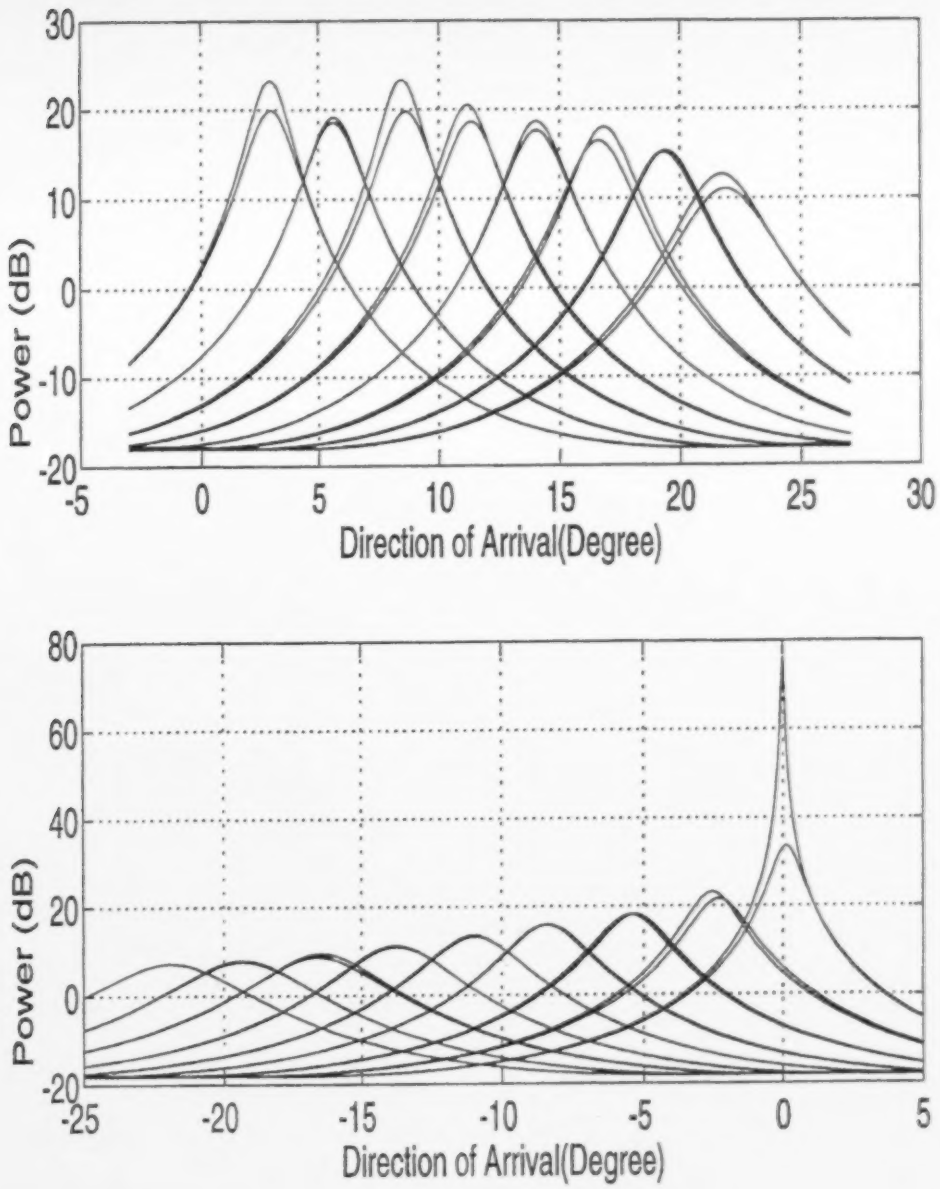

Figure 23: Typical spatial spectra derived using the MUSIC algorithm.

P148620.PDF [Page: 50 of 89]

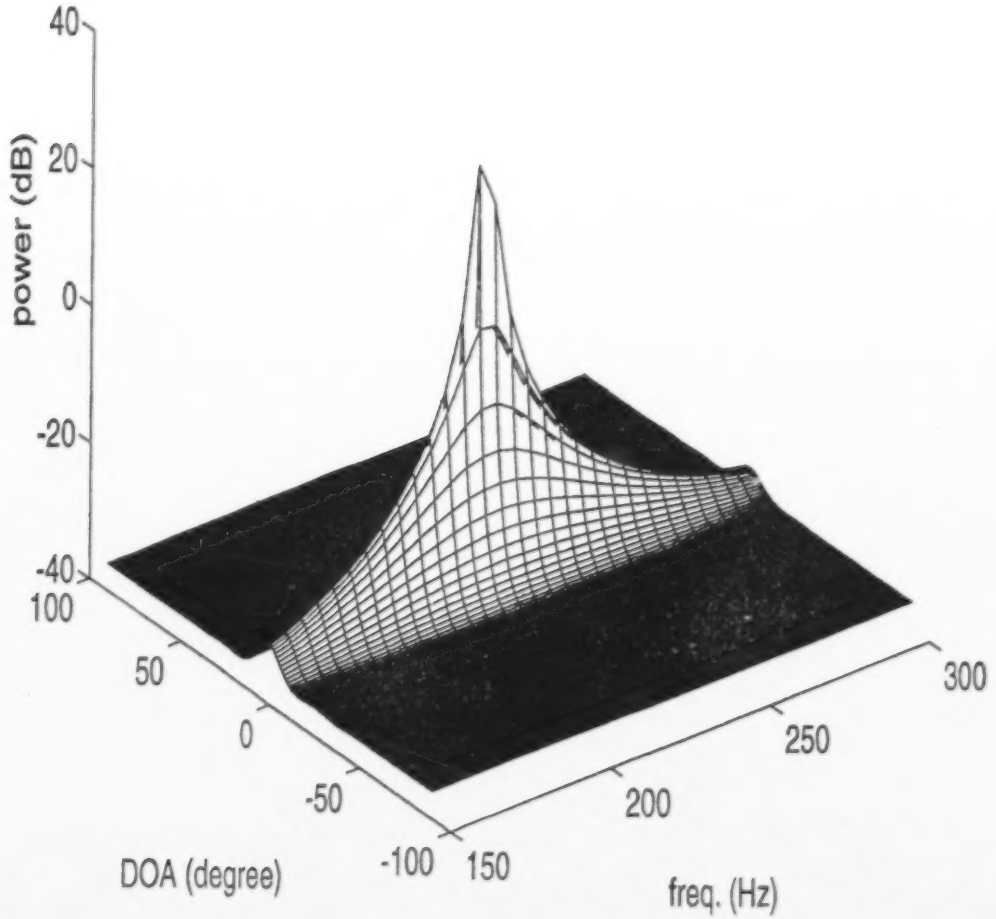

Figure 24: A typical 2-D spatial spectrum derived using the spatio-temporal approach.

tenuation. In the MUSIC case, large deviation begins at 50 dB attenuation. However, there seems to be no effect of nonlinearity at low attenuation. In the case for the spatial-temporal method, there is no significant deviation until the attenuation increased to 70 dB. Furthermore, there is no apparent effect of nonlinearity at low attenuation. For the two-step FBLP method, significant deviation begins at 50 dB attenuation and there are some effects of nonlinearity. Fig. 30 shows the variance of the estimates versus power levels for the four methods. It can be observed that the performance of the DFT method is the poorest amongst the four methods whereas the performance of both the MUSIC and two-step FBLP methods are comparable. At low SNR, the spatio-temporal approach offers the best performance. While the threshold in the performance curves for both the MUSIC and two-step FBLP methods occurs between 40 dB and 50 dB attenuation, the threshold for the spatio-temporal approach occurs between 60 dB and 70 dB attenuation. In this sense, the performance of the spatio-temporal approach is about 20 dB better than the others.

7.3 Mobile Trials

In this subsection the results derived from the data for the far-field moving source are presented. These results were derived using the 2-D DFT, MUSIC, and spatial-temporal methods. In these cases the ability of DF techniques to track the movement of the mobile signal is demonstrated.

7.3.1 Case 1

The automobile with Transmitter 2 travelled from Position 1 to Position 2 (Fig. 2). Data was collected every 50 m along which the vehicle progressed. Figs. 31 to 33 show the DOA estimates derived using the three methods. The dots in the figures represent the DOA estimates for the incoming signals, whereas the small circles represent the calculated angular positions of the automobile. From Figs. 31 it can be observed that when the two sources were close to each other (at the beginning and end of the traces), the DFT technique lost the tracks of one or both of the incoming signals. In contrast, both the MUSIC and spatial-temporal algorithms produced reasonable DOA estimates of the incoming signals. However, all three methods failed when the DOA of the mobile signal was greater than 80° with respect to the array boresight.

7.3.2 Case 2

The automobile with Transmitter 2 travelled from Position 2 to Position 3 (Fig. 2). Data was collected every 50 m along which the vehicle progressed.

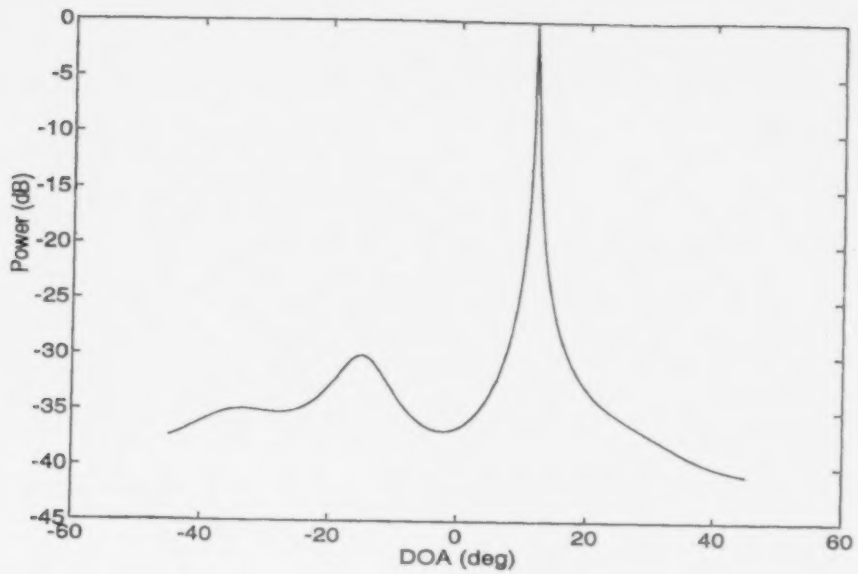

Figure 25: A typical spatial spectrum derived using the two-step FBLP algorithm, DOA=11.3deg.

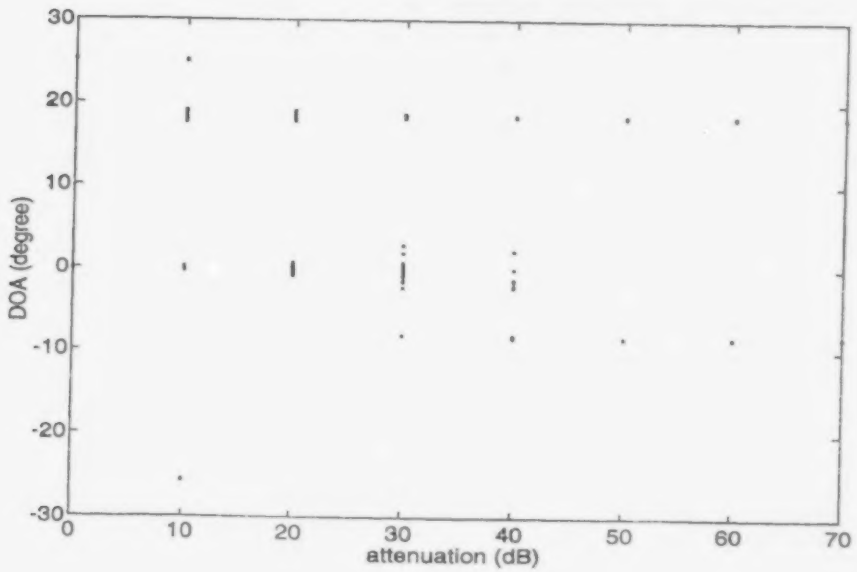

Figure 26: The scattered plot for DOA estimates derived using the 2-D DFT technique.

P148620.PDF [Page: 54 of 89]

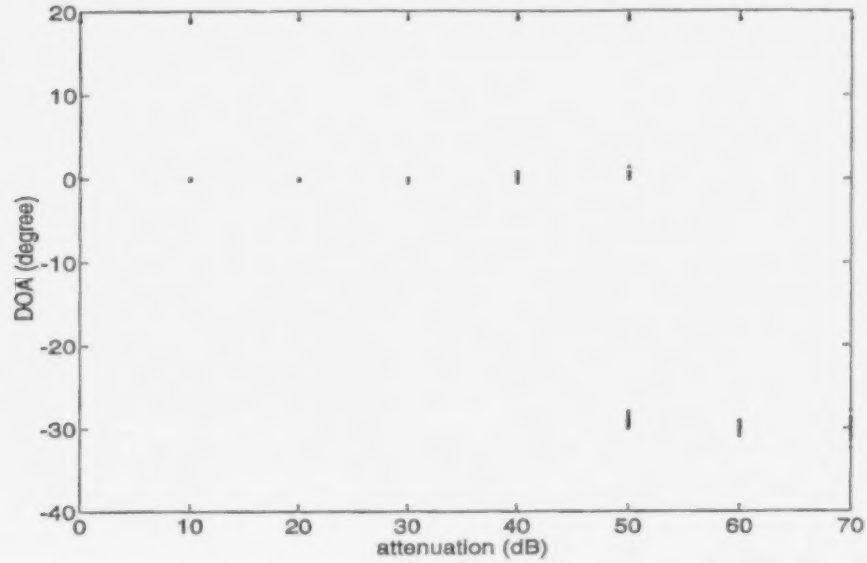

Figure 27: The scattered plot for DOA estimates derived using the MUSIC algorithm.

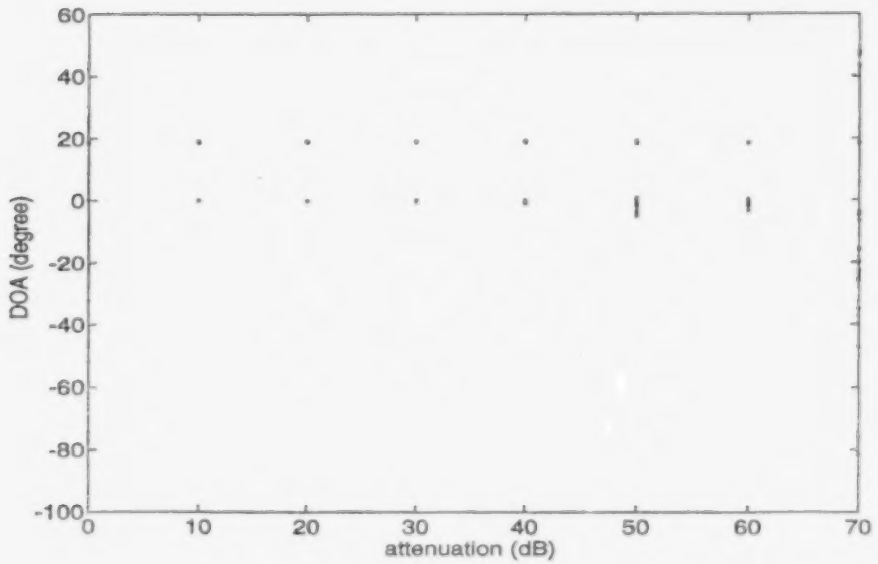

Figure 28: The scattered plot for DOA estimates derived using the spatio-temporal algorithm.

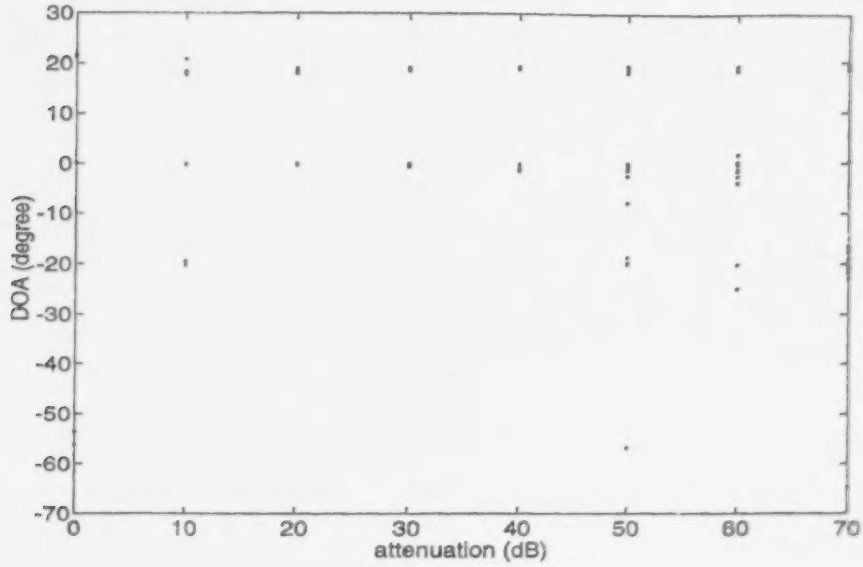

Figure 29: The scattered plot for DOA estimates derived using the two-step FBLP algorithm.

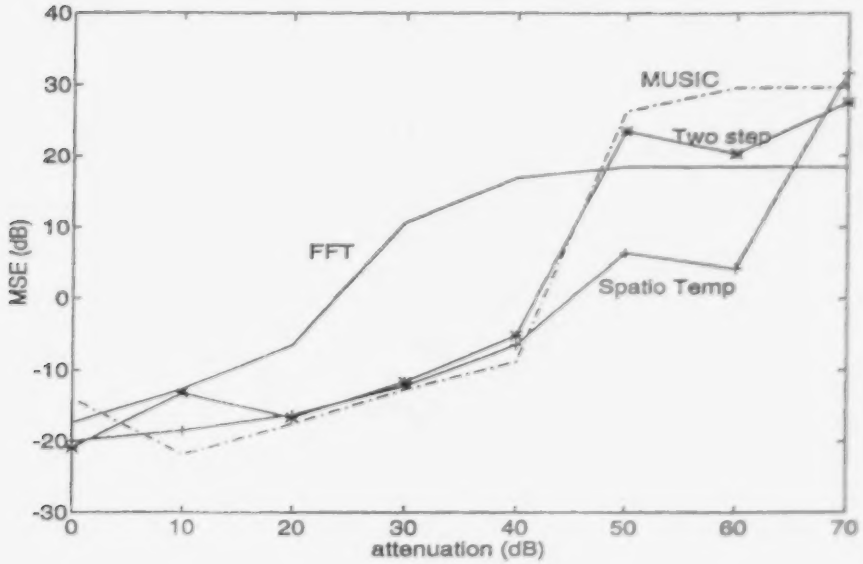

Figure 30: MSE versus signal power level.

P148620.PDF [Page: 56 of 89]

Figs. 34 to 36 show the DOA estimates derived using the three methods. The dots in the figures represent the DOA estimates for the incoming signals, whereas the small circles represent the calculated angular positions of the automobile. Similar observations can be made to those in the first case. That is, when the two signals were angularly close to each other, the DFT technique failed while both the MUSIC and spatial-temporal algorithms produced reasonable DOA estimates of the incoming signals. As well, problems were encountered by all the methods when the DOA of the mobile signal was greater than 80° with respect to the array boresight.

7.3.3 Case 3

The automobile with Transmitter 2 travelled from Position 3 to Position 2 (Fig. 2). Data was collected every 3 to 15 seconds and the vehicle was either moving or stationary. In Figs. 37 to 39 are, respectively, shown the DOA estimates derived using the three methods. These results clearly demonstrate the resolvability of the methods. At the beginning of the trial, the angular direction of the mobile signal with respect to the array boresight changed from positive to negative angles; i.e. the trace of the mobile signal crossed over the trace of the fixed signal. Comparing the three sets of results, one can see that the spatial-temporal approach produced more clear traces at the crossing than the other two methods did. It can be also seen that problems were encountered by all the methods when the DOA of the mobile signal was greater than 80° with respect to the array boresight.

P148620.PDF [Page: 57 of 89]

7.3.4 Case 4

The automobile with Transmitter 2 travelled from Position 4 to Position 5 (Fig. 2). Data was collected every 5 to 10 seconds and the vehicle was either moving or stationary. Figs. 40 to 42 show the DOA estimates derived using the three methods. If in the previous case the results did not clearly demonstrate the superior resolvability of the spatial-temporal approach, the results in this case clearly showed it. For the results derived using the DFT or MUSIC algorithms (Figs. 40 to 41), either the trace for the mobile signal or the trace for the fixed signal was disrupted when the two traces crossed over each other. In contrast, for Fig. 42 it can be seen that the two traces crossed over each other almost without disruption. Again, problems were encountered by all the methods when the DOA of the mobile signal was greater than 80°.

7.3.5 Discussion

In all the four cases, problems were encountered by all the methods when the DOA of the mobile signal was greater than 80° with respect to the array boresight. One reason is that these algorithms are less sensitive to change in signal direction as the signal is closer to $\theta = \pm 90°$. This can easily be seen from the direction vector. The n^{th}element in the direction vector is given by

$$s_n(\theta) = e^{j\frac{2\pi}{\lambda}(n-1)d\sin\theta}. \tag{51}$$

P148620.PDF [Page: 58 of 89]

The derivative of $s_n(\theta)$ with respect to θ gives the sensitivity of $s_n(\theta)$ to the change in θ,

$$s_n'(\theta) = j\frac{2\pi}{\lambda}(n-1)d\cos\theta\ e^{j\frac{2\pi}{\lambda}(n-1)d\sin\theta}. \tag{52}$$

At $\theta = 0$, the sensitivity is

$$s_n'(\theta)_{|\theta=0} = j\frac{2\pi}{\lambda}(n-1)d,$$

whereas the sensitivity at $\theta = 90$ is

$$s_n'(\theta)_{|\theta=90} = 0.$$

Since the algorithms are relatively sensitive to changes in signal direction in the region of boresight, they are relatively less affected by noise. On the other hand, since they are insensitive to changes in signal direction in the end-fire region, they are relatively more susceptible to noise.

P148620.PDF [Page: 59 of 89]

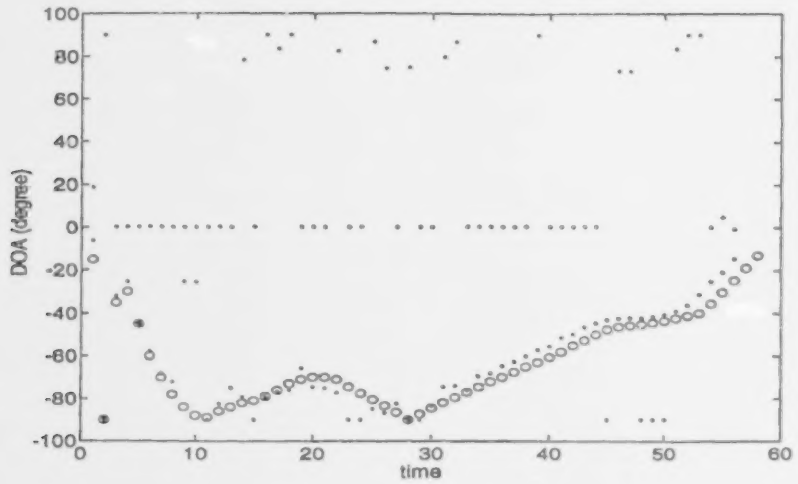

Figure 31: The 2-D DFT DOA results for Case 1.

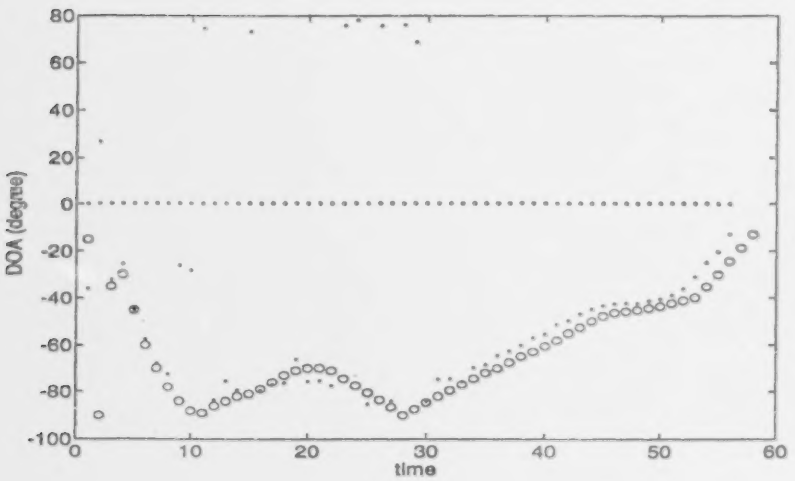

Figure 32: The MUSIC DOA results for Case 1.

P148620.PDF [Page: 60 of 89]

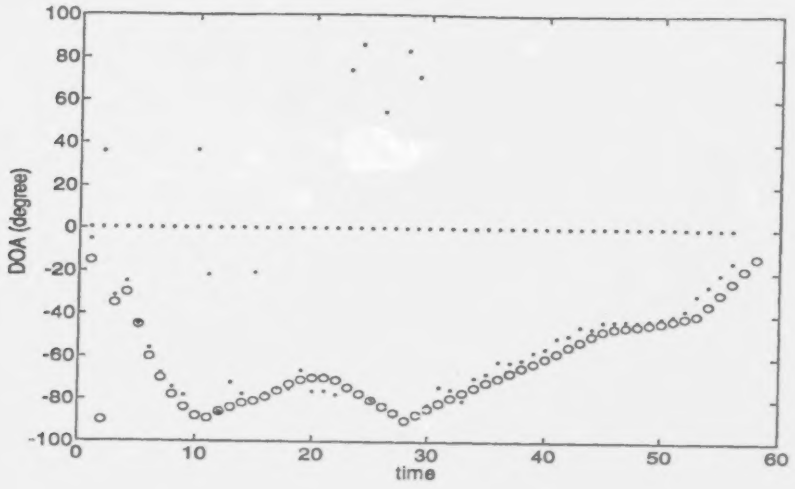

Figure 33: The DOA results derived usin the spatio-temporal method for Case 1.

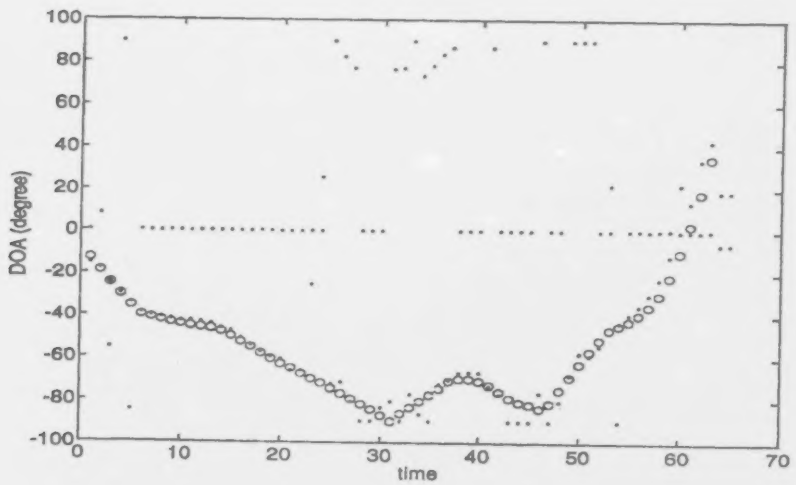

Figure 34: The 2-D DFT DOA results for Case 2.

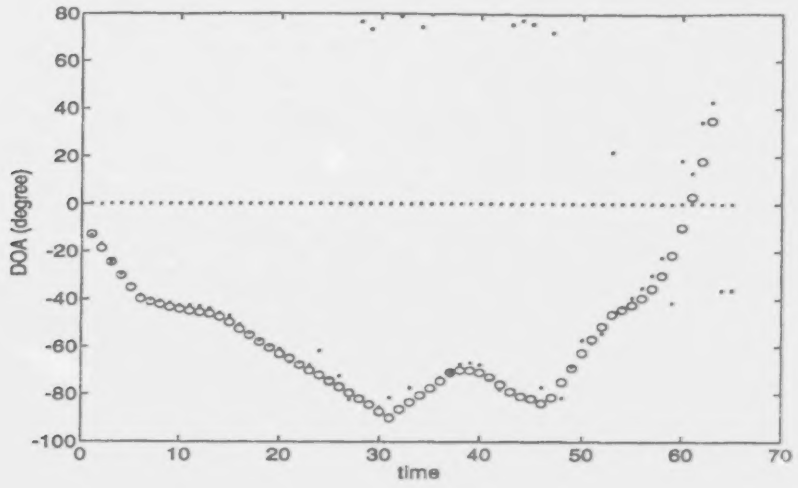

Figure 35: The MUSIC DOA results for Case 2.

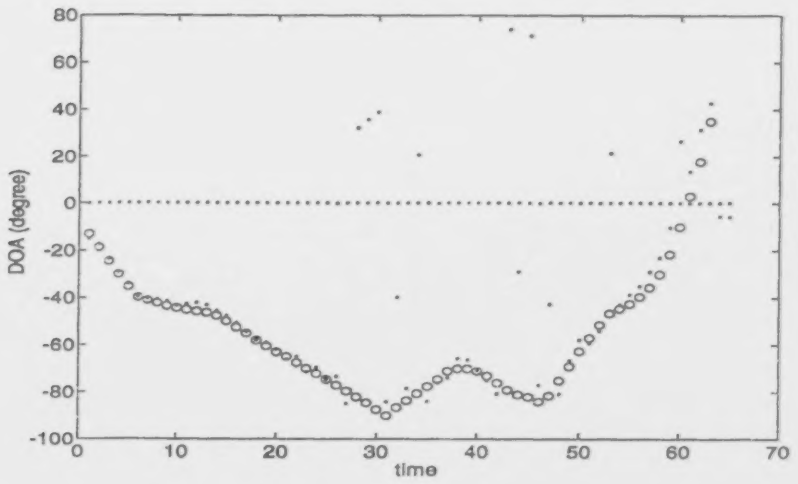

Figure 36: The DOA results derived usin the spatio-temporal method for Case 2.

P148620.PDF [Page: 62 of 89]

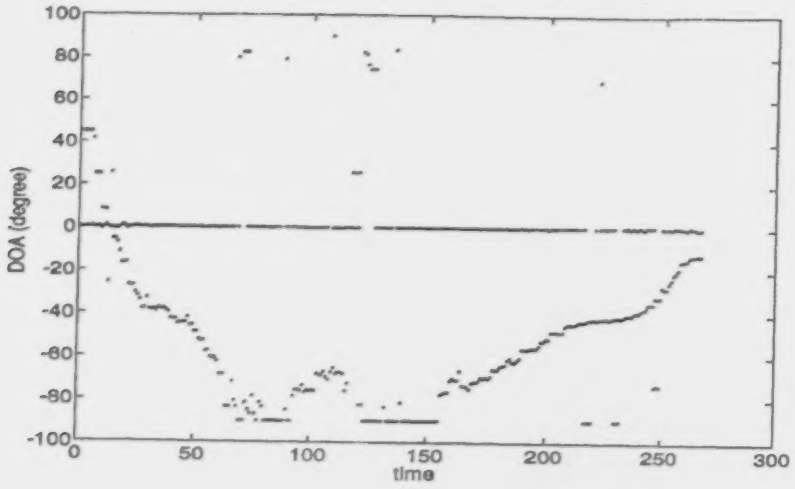

Figure 37: The 2-D DFT DOA results for Case 3.

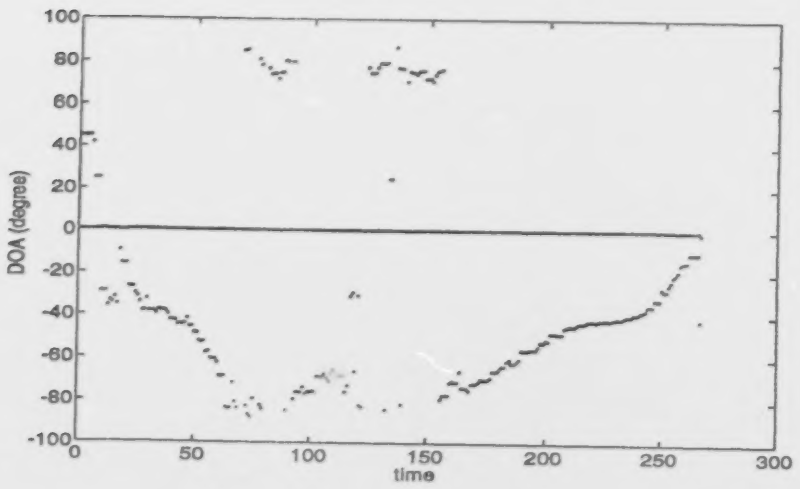

Figure 38: The MUSIC DOA results for Case 3.

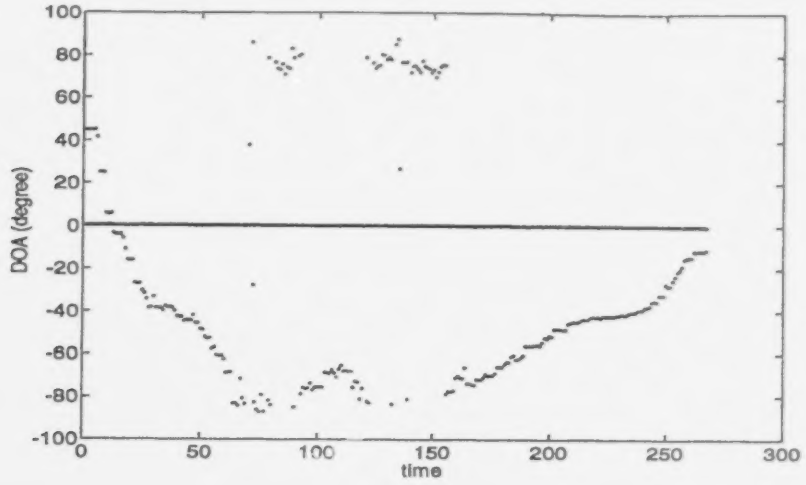

Figure 39: The DOA results derived usin the spatio-temporal method for Case 3.

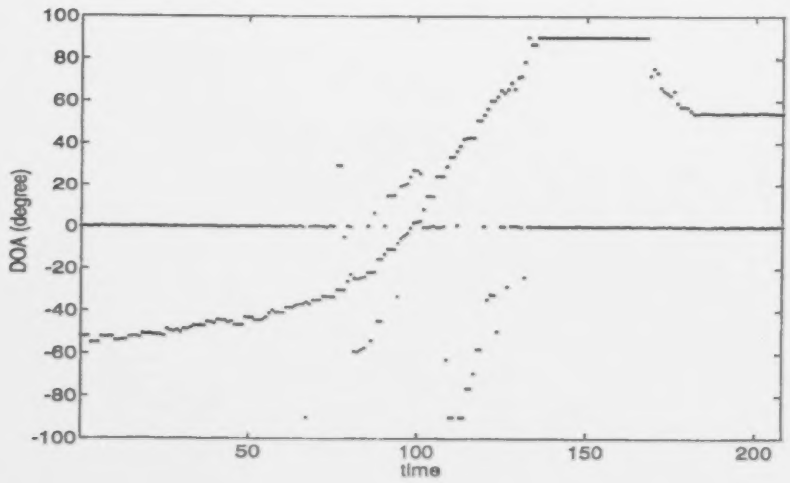

Figure 40: The 2-D DFT DOA results for Case 4.

P148620.PDF [Page: 64 of 89]

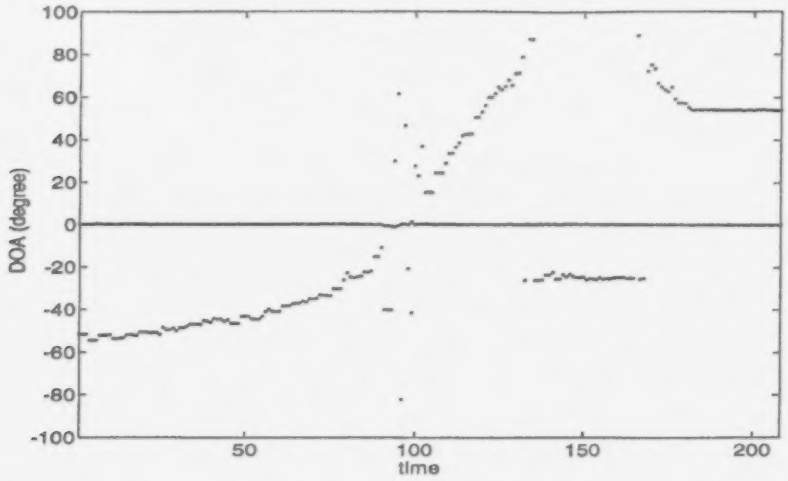

Figure 41: The MUSIC DOA results for Case 4.

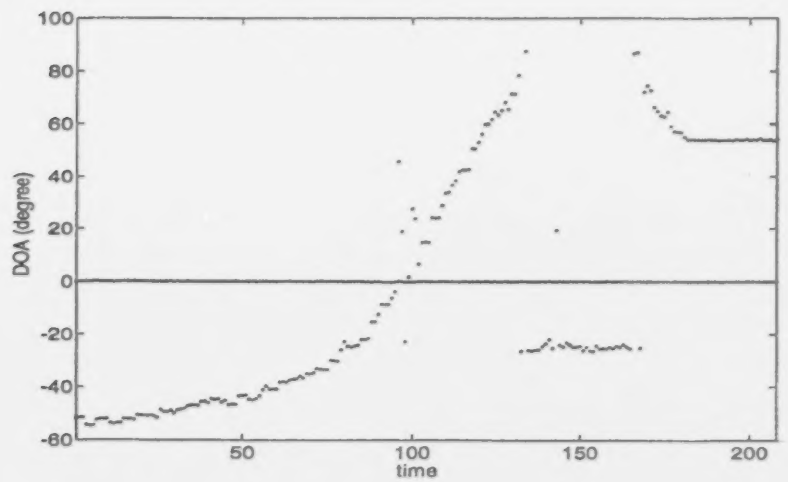

Figure 42: The DOA results derived usin the spatio-temporal method for Case 4.

P148620.PDF [Page: 65 of 89]

8 Conclusions and Recommendations

In this report, we have described the experimental trials to establish a DF database in a multipath environment using an advanced eight-element DF system. Based on the collected data, the development of a signal model and the study of the characteristics of the multipath signals were carried out . Furthermore, a number of direction-of-arrival algorithms have been investigated and their performance has also been evaluated based on the real data.

8.1 Findings

Based on the analysis results, the following observations have been made:

1. It was found that for the near-field case, there are relatively strong temporal and spatial correlations in the array data. As well, significant peaks are observed at low frequency in the spectrum. On the other hand, much less correlations can be seen for the far field case and there is no significant peak in the spectrum.

2. It was observed that the performance of the DFT method was the poorest amongst the four methods whereas the performance of both the MUSIC and two-step FBLP methods was comparable. At low SNR, the spatio-temporal approach offered the best performance. While the threshold in the performance curves for both the MUSIC and two-step FBLP methods occurred between 40 dB and 50 dB attenuation, the

P148620.PDF [Page: 66 of 89]

threshold for the spatio-temporal approach occurred between 60 dB and 70 dB attenuation. In this sense, the performance of spatio-temporal approach was about 20 dB better than the others.

3. It was found, based on the mobile trials, that the ability of the spatio-temporal approach to resolve two closely spaced signals was superior to that of the other techniques.

4. It was found that problems were encountered by all the methods when the DOA of the mobile signal was greater than 80° with respect to the array boresight. One reason is that since the algorithms are relatively sensitive to changes in signal direction in the region of boresight, they are relatively less affected by noise. On the other hand, since they are insensitive to changes in signal direction in the end-fire region, they are relatively more susceptible to noise.

8.2 Recommendations

Based on the observations and findings, a number of recommendations are made for future research.

1. Every method has its own limitations. Undesirably, the spatio-temporal method has higher computational load than the other methods do. Therefore, a study may be carried out to reduce the computational load while the performance is maintained at the same level.

2. A fair amount of information has been obtained from the data that we have collected so far. However, since these measurements were not

carried out in a controlled environment, many parameters remained unknown. Thus, it is difficult to construct a complete mathematical signal model for the multipath phenomena. If a relatively comprehensive model is desirable, it is believed that model experiments may be required.

3. One main objective of the DF system is to intercept communications signals from objects of interest. The communications can be in any format of modulation (e.g, AM & FM) and any format of coding (e.g. spread spectrum). The analysis that we have carried out was based on narrow band signals. Therefore, it may be desirable to investigate the effects that multipath propagation of wide-band signals has on a DF system.

References

[1] J. Litva and L.Lai, "Multipath measurement and modelling," CRL Report No. 255, McMaster University, July 1992.

[2] R. Schmidt, "Multiple Emitter Location and Signal Parameter Estimation," Proc. of the RADC Spectrum Estimation Workshop, RADC-TR-79-63, Rome Air Development Centre, Rome , N.Y., Oct. 1979.

P148620.PDF [Page: 68 of 89]

Appendix

A Results of Multipath Analysis

P148620.PDF [Page: 69 of 89]

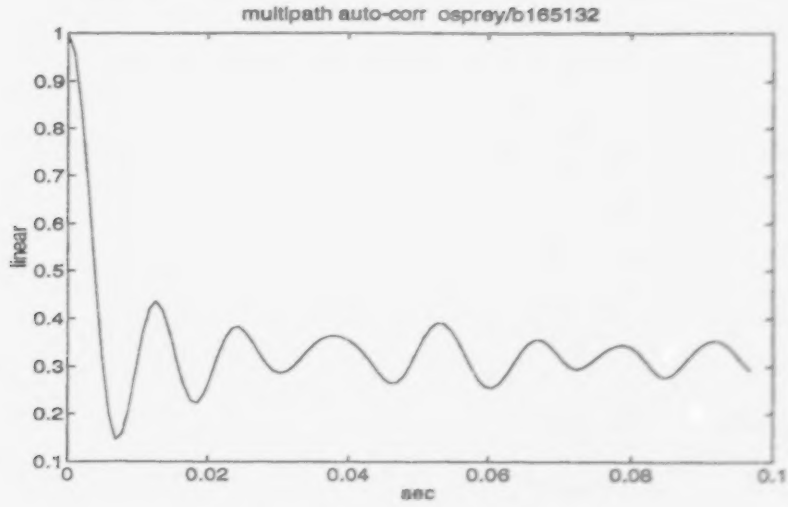

Figure 43: Temporal auto-correlation function of the near-field multipath signal.

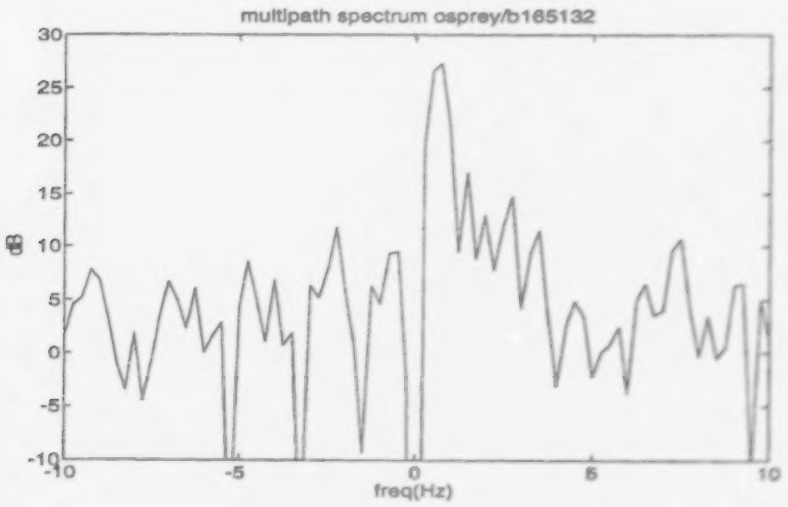

Figure 44: Power spectrum of the near-field multipath multipath signals.

P148620.PDF [Page: 70 of 89]

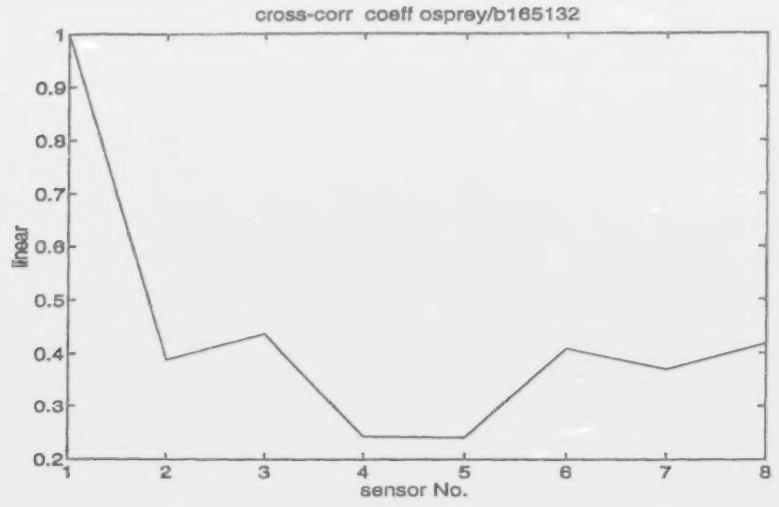

Figure 45: Cross-correlation coefficients of the near-field multipath signals.

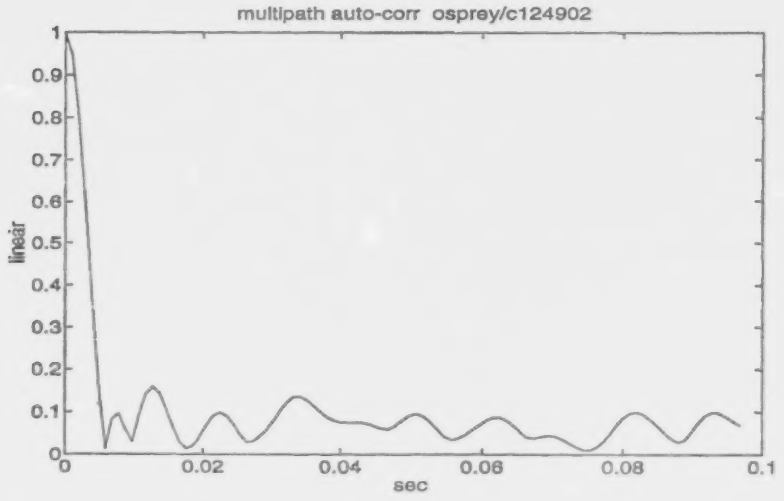

Figure 46: Temporal auto-correlation function of the near-field multipath signal.

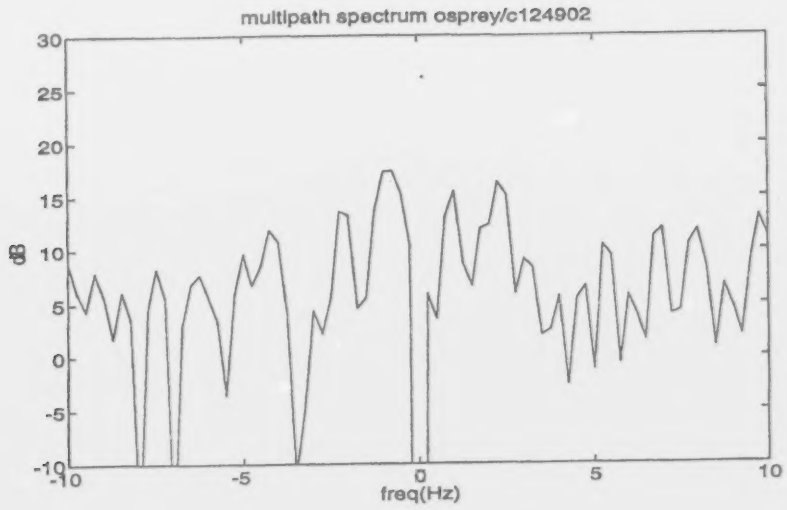

Figure 47: Power spectrum of the near-field multipath multipath signals.

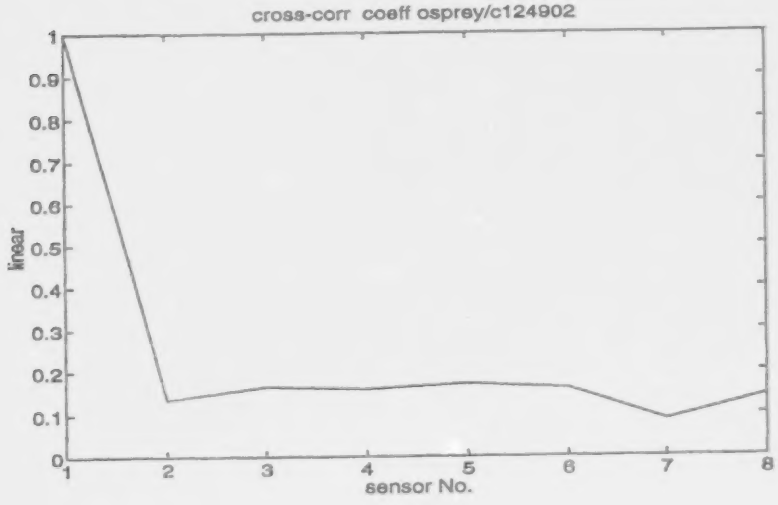

Figure 48: Cross-correlation coefficients of the near-field multipath signals.

P148620.PDF [Page: 72 of 89]

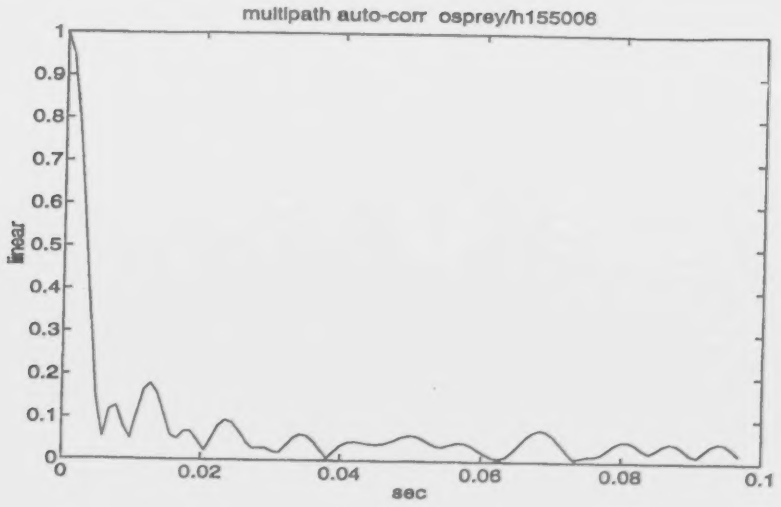

Figure 49: Temporal auto-correlation function of the far-field multipath signal.

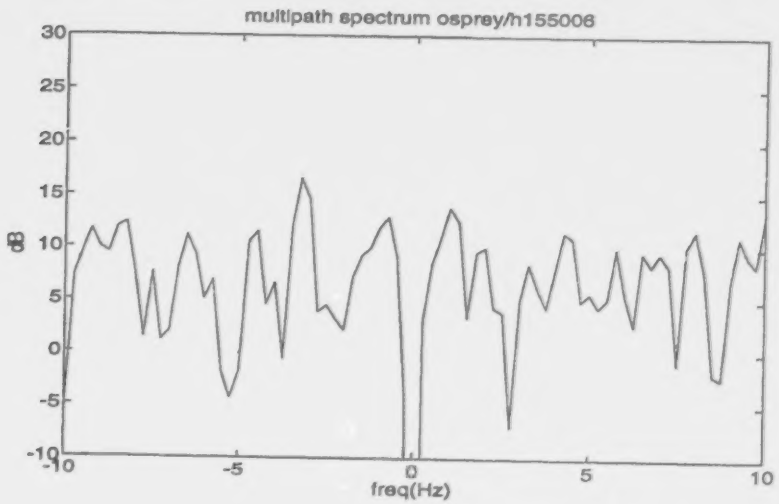

Figure 50: Power spectrum of the far-field multipath multipath signals.

P148620.PDF [Page: 73 of 89]

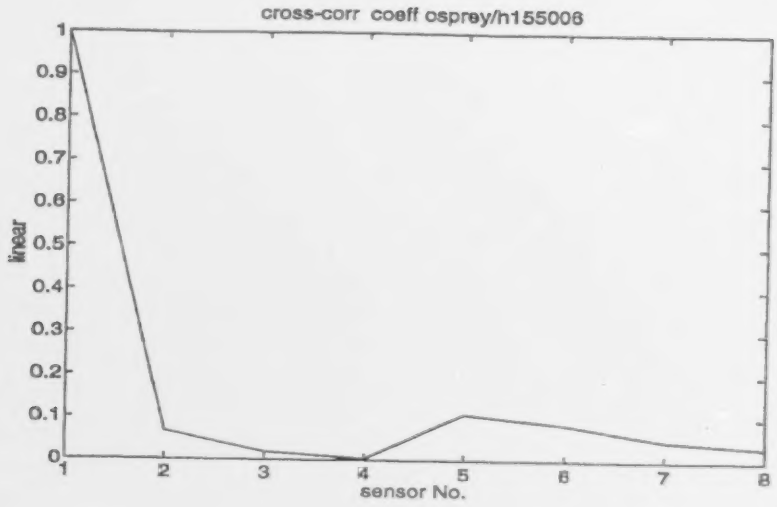

Figure 51: Cross-correlation coefficients of the far-field multipath signals.

P148620.PDF [Page: 74 of 89]

B DOA Results

P148620.PDF [Page: 75 of 89]

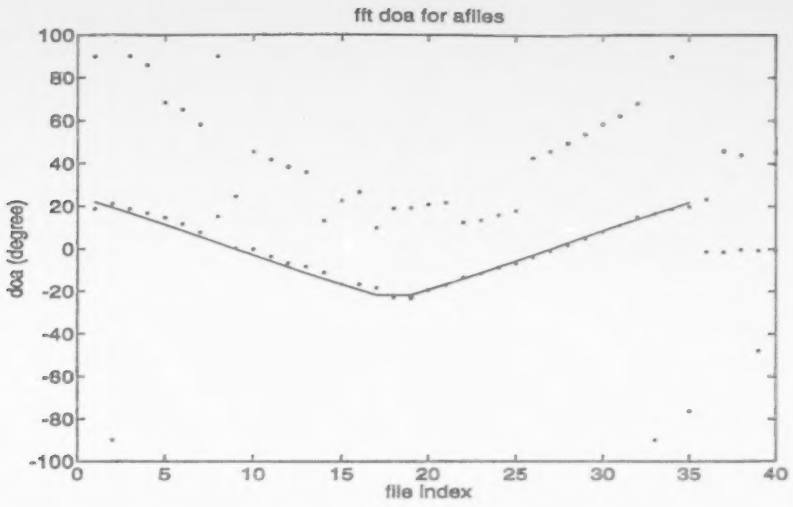

Figure 52: The 2-D DFT DOA estimates for a-files (Mar. 1993).

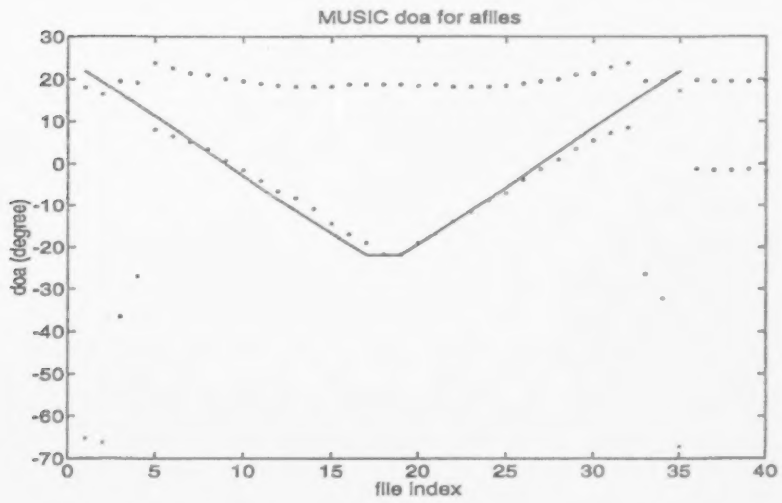

Figure 53: The MUSIC DOA estimates for a-files (Mar. 1993).

P148620.PDF [Page: 76 of 89]

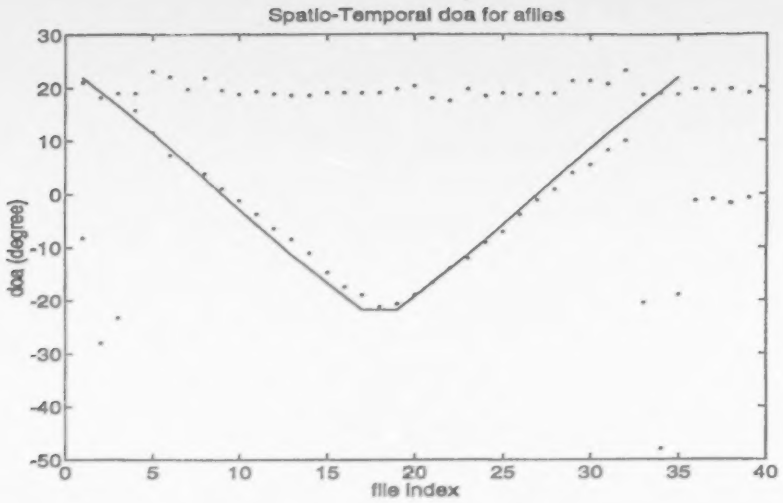

Figure 54: The spatio-temporal DOA estimates for a-files (Mar. 1993).

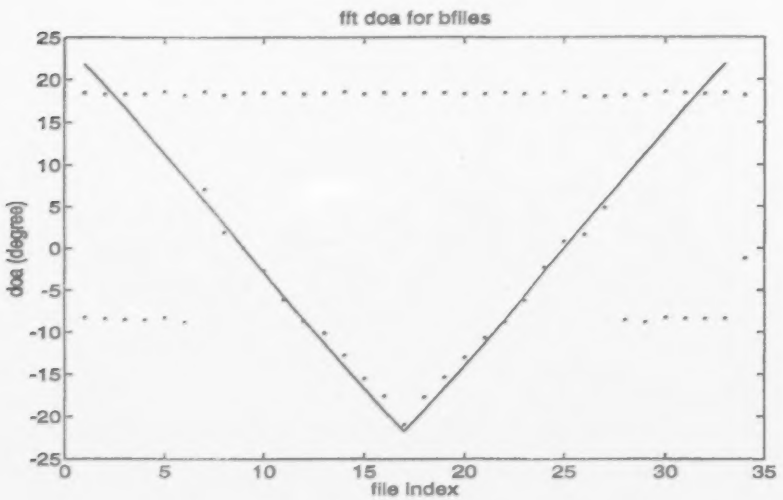

Figure 55: The 2-D DFT DOA estimates for b-files (Mar. 1993).

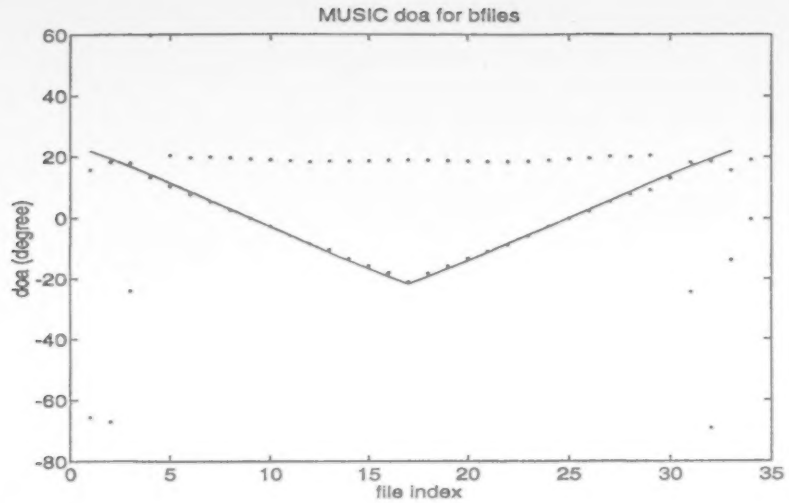

Figure 56: The MUSIC DOA estimates for b-files (Mar. 1993).

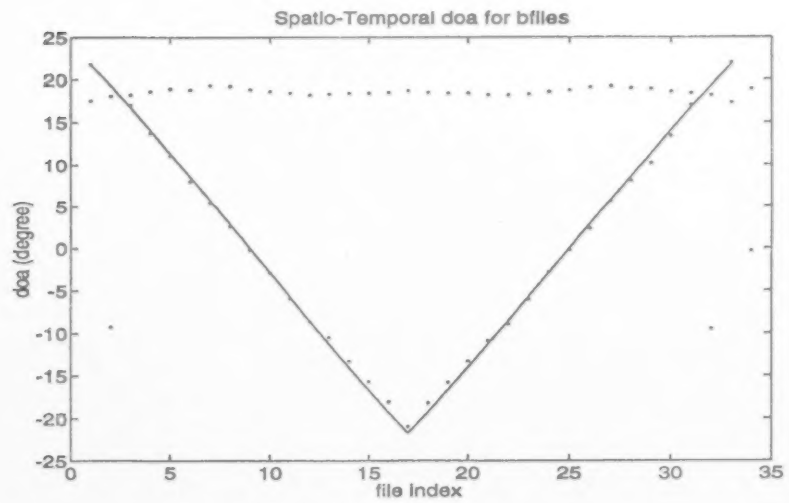

Figure 57: The spatio-temporal DOA estimates for b-files (Mar. 1993).

P148620.PDF [Page: 78 of 89]

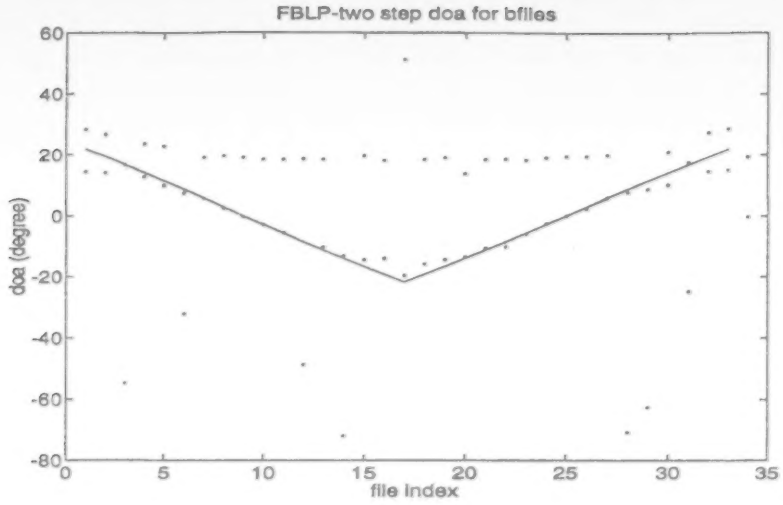

Figure 58: The two-step FBLP DOA estimates for b-files (Mar. 1993).

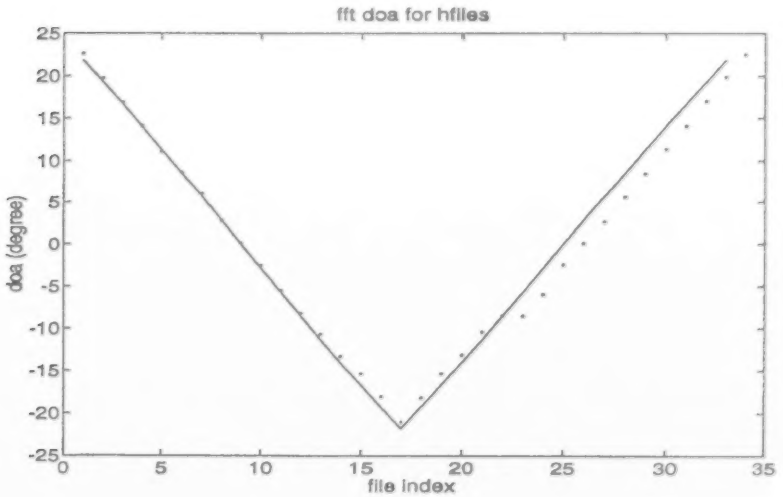

Figure 59: The 2-D DFT DOA estimates for h-files (Mar. 1993).

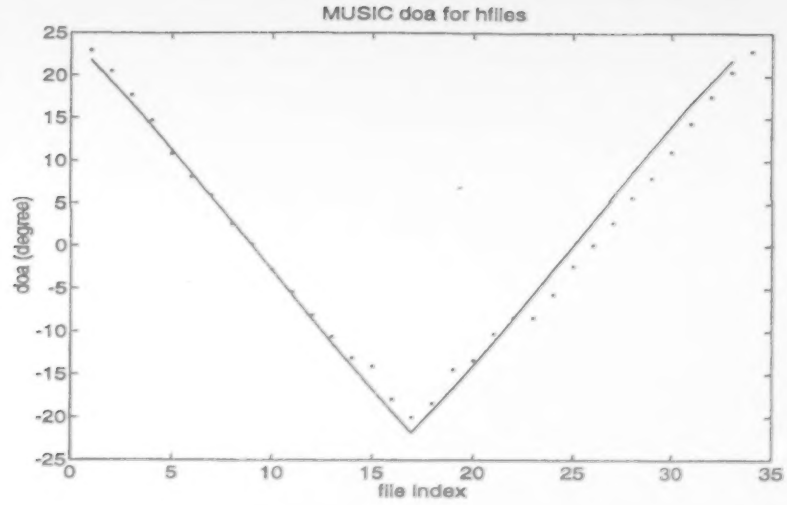

Figure 60: The MUSIC DOA estimates for h-files (Mar. 1993).

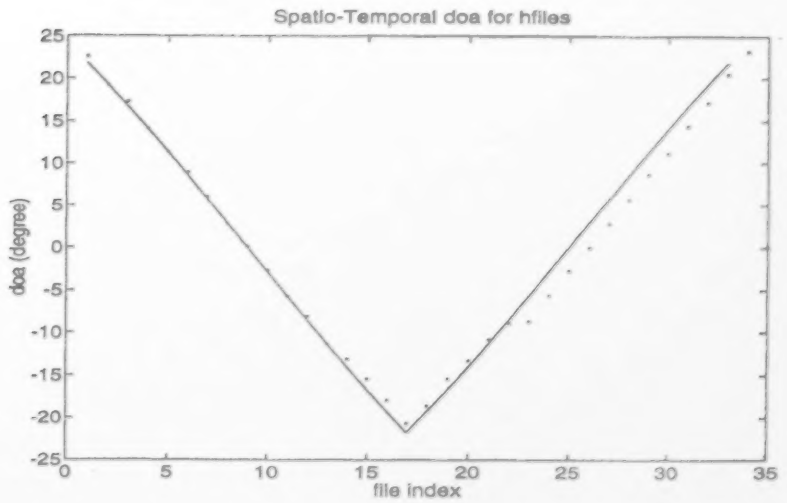

Figure 61: The spatio-temporal DOA estimates for h-files (Mar. 1993).

P148620.PDF [Page: 80 of 89]

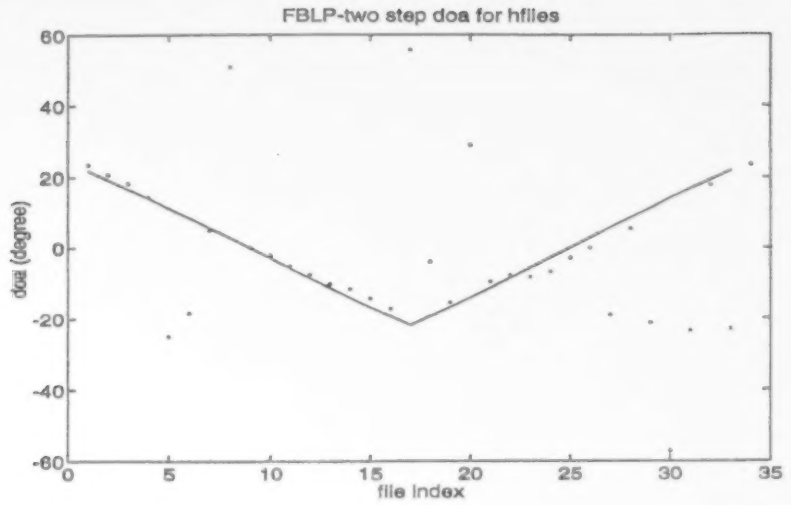

Figure 62: The two-step FBLP DOA estimates for h-files (Mar. 1993).

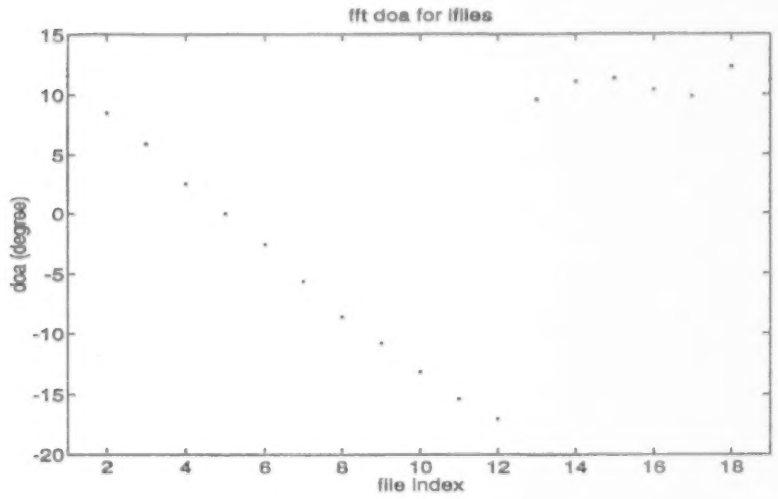

Figure 63: The 2-D DFT DOA estimates for i-files (Mar. 1993).

P148620.PDF [Page: 81 of 89]

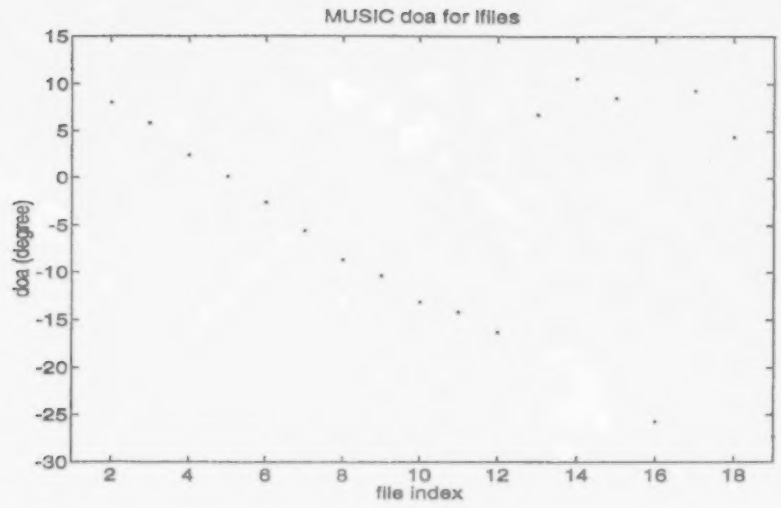

Figure 64: The MUSIC DOA estimates for i-files (Mar. 1993).

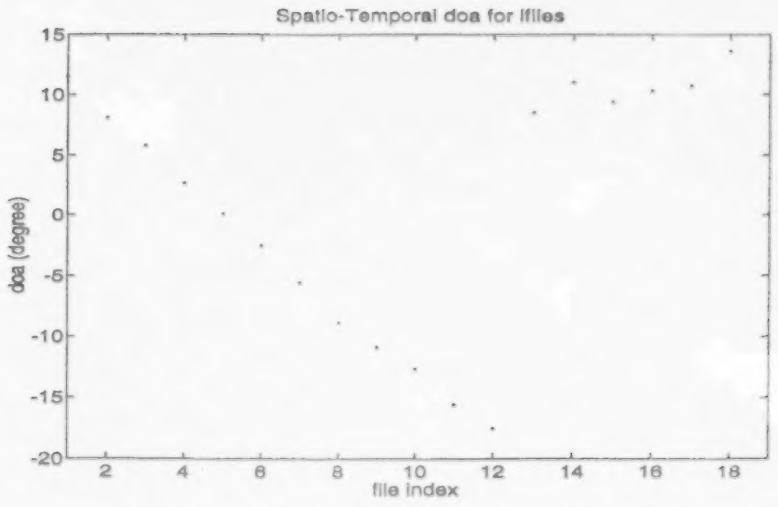

Figure 65: The spatio-temporal DOA estimates for i-files (Mar. 1993).

P148620.PDF [Page: 82 of 89]

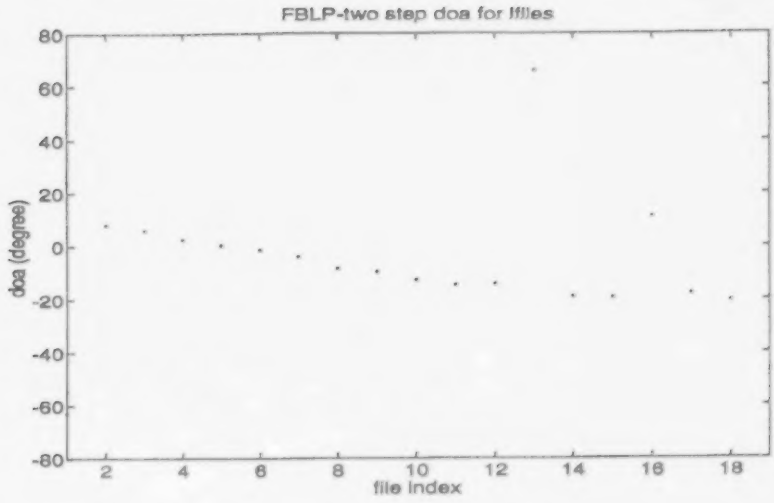

Figure 66: The two-step FBLP DOA estimates for i-files (Mar. 1993).

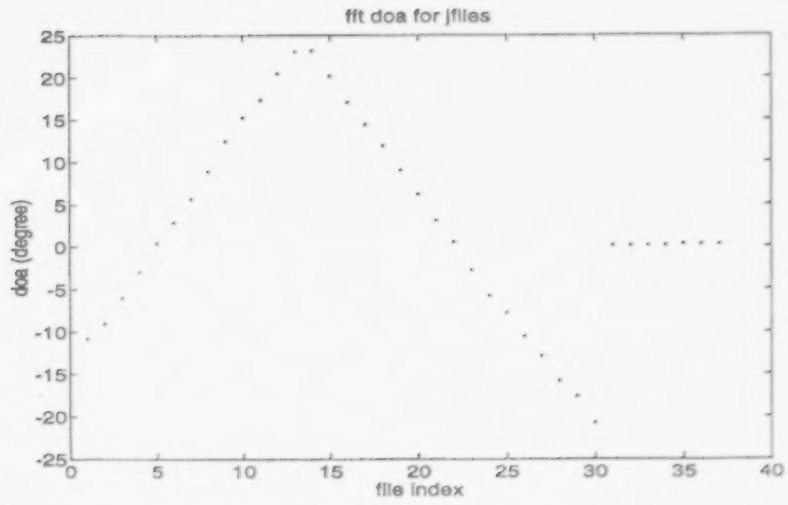

Figure 67: The 2-D DFT DOA estimates for j-files (Mar. 1993).

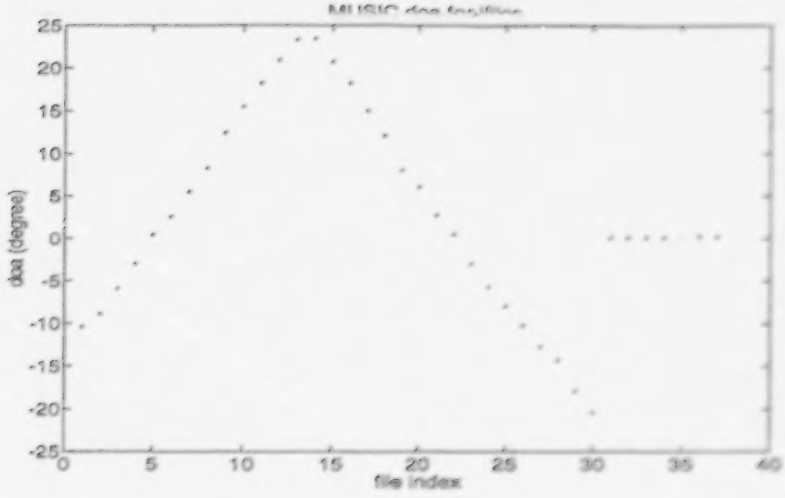

Figure 68: The MUSIC DOA estimates for j-files (Mar. 1993).

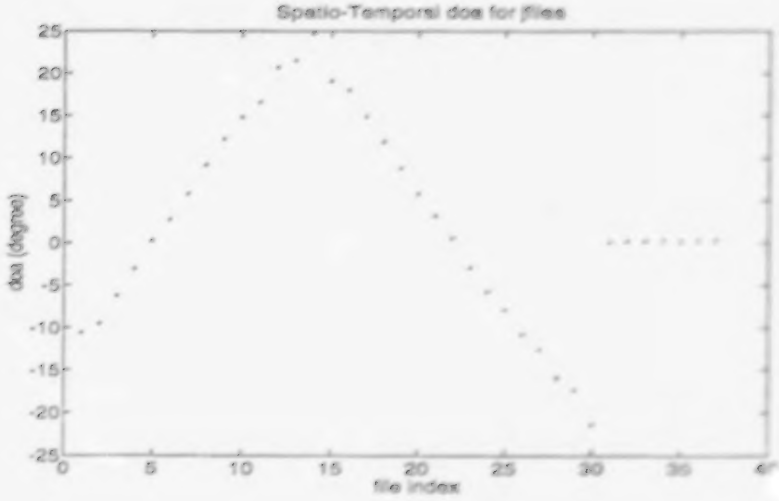

Figure 69: The spatio-temporal DOA estimates for j-files (Mar. 1993).

P148620.PDF [Page: 84 of 89]

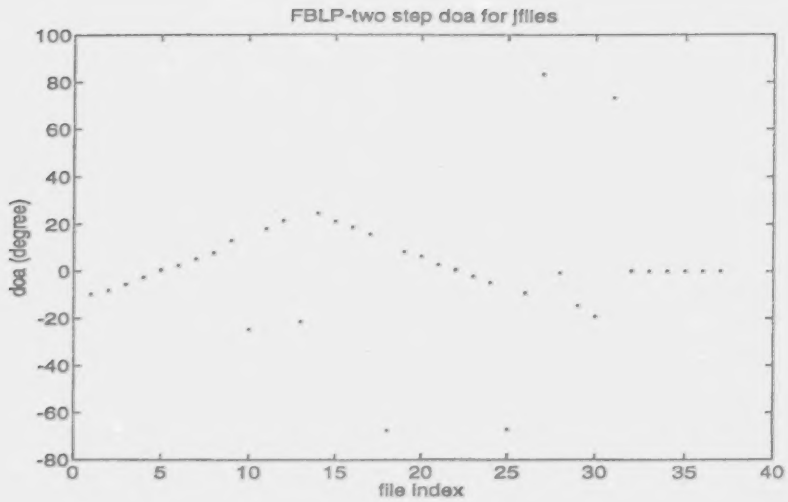

Figure 70: The two-step FBLP DOA estimates for j-files (Mar. 1993).

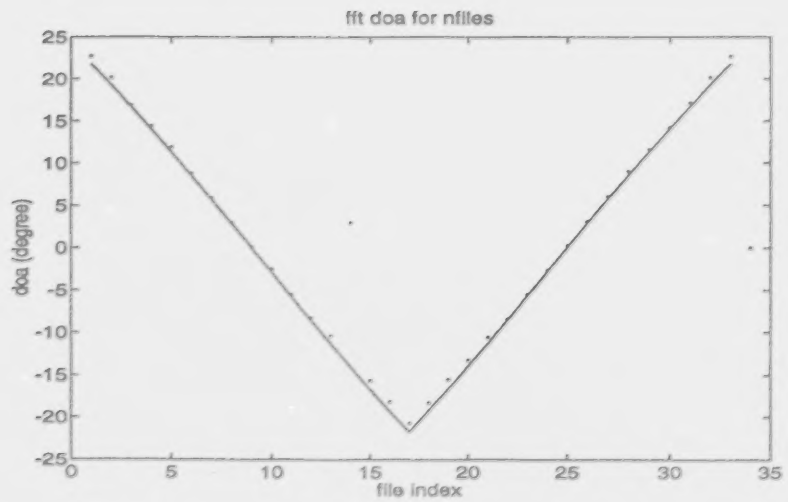

Figure 71: The 2-D DFT DOA estimates for n-files (Mar. 1993).

P148620.PDF [Page: 85 of 89]

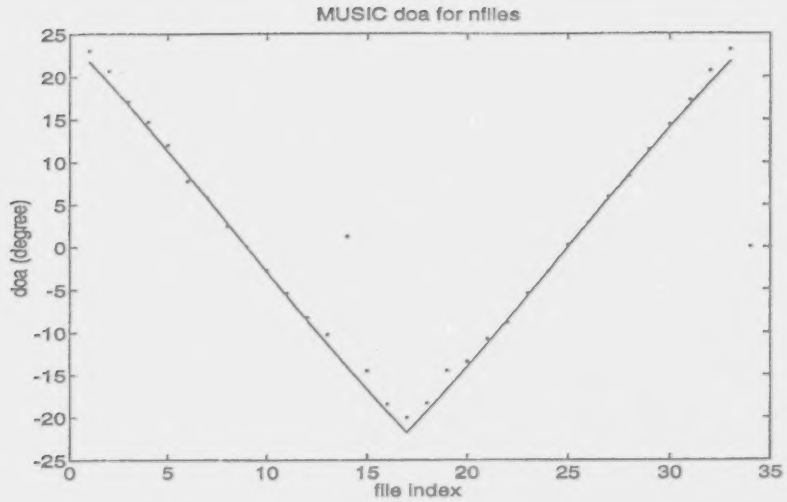

Figure 72: The MUSIC DOA estimates for n-files (Mar. 1993).

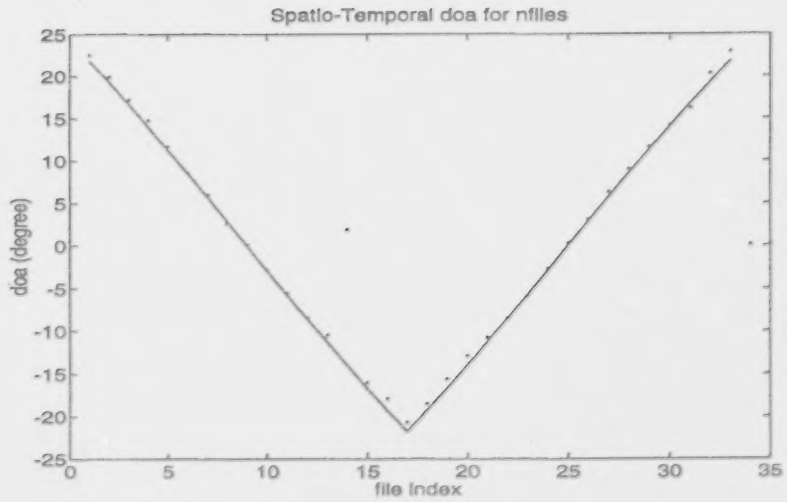

Figure 73: The spatio-temporal DOA estimates for n-files (Mar. 1993).

P148620.PDF [Page: 86 of 89]

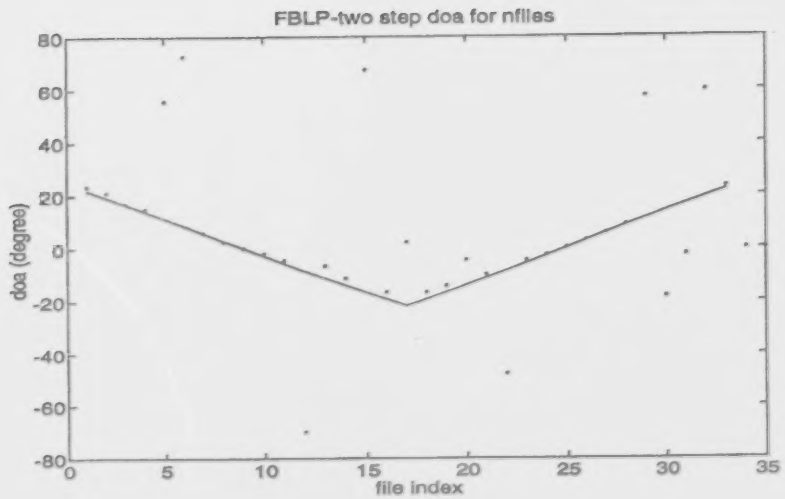

Figure 74: The two-step FBLP DOA estimates for n-files (Mar. 1993).

13. ABSTRACT (a brief and factual summary of the document. It may also appear elsewhere in the body of the document itself. It is highly desirable that the abstract of classified documents be unclassified. Each paragraph of the abstract shall begin with an indication of the security classification of the information in the paragraph (unless the document itself is unclassified) represented as (S), (C), or (U). It is not necessary to include here abstracts in both offical languages unless the text is bilingual).

(U) This report is a part of the ongoing research that has been carried out by DREO and CRL to study the multipath effects on a direction finding (DF) system. The present project has been to establish a real DF database and to carry out a comprehensive analysis of the data. A highly advanced eight-element DF system has been used to collect field trial data. Based on the collected data, the development of signal model and the study of the characteristics of the multipath signals were carried out. Furthermore, a number of direction-of-arrival algorithms have been investigated and their performance has also been evaluated based on the real data. This report consists of the following parts:

1. experimental trials
2. signal modelling
3. data calibration
4. analysis of signal characteristics
5. development and investigation of practical techniques for direction finding
6. DF performance evaluation.

Based on the observations and findings during the course of this work, a number of recommendations are made for future research.

14. KEYWORDS, DESCRIPTORS or IDENTIFIERS (technically meaningful terms or short phrases that characterize a document and could be helpful in cataloguing the document. They should be selected so that no security classification is required. Identifiers, such as equipment model designation, trade name, military project code name, geographic location may also be included. If possible keywords should be selected from a published thesaurus. e.g. Thesaurus of Engineering and Scientific Terms (TEST) and that thesaurus-identified. If it is not possible to select indexing terms which are Unclassified, the classification of each should be indicated as with the title.)

DIRECTION FINDING
DIRECTION-OF-ARRIVAL ESTIMATION
VHF
MULTIPATH
MUSIC
LINEAR PREDICTION
SUPERRESOLUTION
SPATIO-TEMPORAL SPECTRAL ANALYSIS
DIGITAL BEAMFORMING

P148620.PDF [Page: 88 of 89]

UNCLASSIFIED

SECURITY CLASSIFICATION OF FORM
(highest classification of Title, Abstract, Keywords)

DOCUMENT CONTROL DATA

(Security classification of title, body of abstract and indexing annotation must be entered when the overall document is classified)

1. ORIGINATOR (the name and address of the organization preparing the document. Organizations for whom the document was prepared, e.g. Establishment sponsoring a contractor's report, or tasking agency, are entered in section 8.)

MCMASTER UNIVERSITY

2. SECURITY CLASSIFICATION (overall security classification of the document. including special warning terms if applicable)

UNCLASSIFIED

3. TITLE (the complete document title as indicated on the title page. Its classification should be indicated by the appropriate abbreviation (S,C or U) in parentheses after the title.)

HIGH ACCURACY DIRECTION FINDING TRIALS (U)

4. AUTHORS (Last name, first name, middle initial)

T. LO, F. WANG AND J. LITVA

5. DATE OF PUBLICATION (month and year of publication of document)

NOVEMBER 1993

6a. NO. OF PAGES (total containing information. Include Annexes, Appendices, etc.)

82

6b. NO. OF REFS (total cited i document)

2

7. DESCRIPTIVE NOTES (the category of the document, e.g. technical report, technical note or memorandum. If appropriate, enter the type c report, e.g. interim, progress, summary, annual or final. Give the inclusive dates when a specific reporting period is covered.)

CONTRACTOR REPORT - FINAL

8. SPONSORING ACTIVITY (the name of the department project office or laboratory sponsoring the research and development. Include the address.)

DEFENCE RESEARCH ESTABLISHMENT OTTAWA
NATIONAL DEFENCE
SHIRLEY BAY, OTTAWA, ONTARIO K1A 0K2 CANADA

9a. PROJECT OR GRANT NO. (if appropriate, the applicable research and development project or grant number under which the document was written. Please specify whether project or grant)

041LX

9b. CONTRACT NO. (if appropriate, the applicable number under which the document was written)

W7714-2-9691

10a. ORIGINATOR'S DOCUMENT NUMBER (the official document number by which the document is identified by the originating activity. This number must be unique to this document.)

CRL REPORT NO. 273

10b. OTHER DOCUMENT NOS. (Any other numbers which may be assigned this document either by the originator or by the sponsor)

11. DOCUMENT AVAILABILITY (any limitations on further dissemination of the document, other than those imposed by security classification

(XX) Unlimited distribution
( ) Distribution limited to defence departments and defence contractors; further distribution only as approved
( ) Distribution limited to defence departments and Canadian defence contractors; further distribution only as approved
( ) Distribution limited to government departments and agencies; further distribution only as approved
( ) Distribution limited to defence departments; further distribution only as approved
( ) Other (please specify):

12. DOCUMENT ANNOUNCEMENT (any limitation to the bibliographic announcement of this document. This will normally correspond to the Document Availabilty (11). However, where further distribution (beyond the audience specified in 11) is possible, a wider announcement audience may be selected.)

UNLIMITED

UNCLASSIFIED

SECURITY CLASSIFICATION OF FORM

Defence Research and Development Canada | Recherche et développement pour la défense Canada

Canada

Français | Contact Us | Help | Search | Canada Site
Home | Defence R&D Canada | Defence Site

Browse Indexes

Titles

Authors

Descriptors

Corporate Authors

Corporate Acronyms

Report Numbers

Search Database

Summary

It is recommended you search "Authors" and "Corporate Authors" on their respective "Browse" pages.

Click here if you are having problems displaying text (ie. text is too big, or too small) or page appears to be jumbled.

Prior Top **Document:** 1 of 1 Bottom Next Click here to Order Click here to Download

TITLE:(U) HIGH ACCURACY DIRECTION FINDING TRIALS

PERSONAL AUTHOR: Lo, T.; Wang, F.; Litva, J.

CORPORATE AUTHOR: McMaster Univ, Hamilton ONT (CAN) Communications Research Lab;Defence Research Establishment Ottawa, Ottawa ONT (CAN)

ABSTRACT: (U) The report is a part of the ongoing research that has been carried out by DREO and CRL to study the multipath effects on a direction finding (DF) system. The present project has been to establish a real DF database and to carry out a comprehensive analysis of the data. A highly advanced eight-element DF system has been used to collect field trial data. Based on the collected data, the development of signal model and the study of the characteristics of the multipath signals were carried out. Furthermore, a number of direction-of-arrival algorithms have been investigated and their performance has also been evaluated based on the real data. The report consists of the following parts: 1. experimental trials; 2. signal modelling; 3. data calibration; 4. analysis of signal characteristics; 5. development and investigation of practical techniques for direction finding; 6. DF performance evaluation. Based on the observations and findings during the course of this work, a number of recommendations are made for future research.

DESCRIPTORS: (U) Direction finding;DOA (Direction of arrival);Very high frequencies;Multipath transmission;Field tests;Calibrating;Signal processing;Data bases

IDENTIFIERS: (U) MUSIC;Linear prediction;Superresolution;Spatio-temporal spectral analysis;Digital beamforming

REPORT NUMBER: CRL-273; Contractor Report (Final)

REPORT DATE: 01 Nov 1993

NUMBER OF PAGES : 85

DRDKIM N°: 95-00952

CANDIS N°: 148620

Format(s): Hardcopy;Document Image stored on Optical Disk

Date modified: 2003-04-17

Important Notices